

High-Speed Astrophysics: Rapid Events Near Compact Binaries

Helena Uthas

Lund Observatory
Lund University



2005-EXA06

Degree project of 20 credit points (for a degree of Master)
April 2005

Lund Observatory
Box 43
SE-221 00 Lund
Sweden

High-Speed Astrophysics

Rapid Events Near Compact Binaries



Helena Uthas
Lund Observatory
2005

Contents

1	Introduction	5
1.1	What is High-Speed Astrophysics? (HSA)	5
1.2	Where are High-Speed Phenomena Present?	5
1.3	How Can these Rapid Phenomena be Detected?	6
1.4	High-Speed Astrophysics at Lund Observatory	7
2	Astrophysical Challenges	9
2.1	Introduction	9
2.1.1	What is a Quasi-Periodic Oscillation?	10
2.2	Cataclysmic Variables and their Rapid Phenomena	10
2.2.1	The Search for High-Speed Events in Cataclysmic Variables	10
2.2.2	What is a Cataclysmic Variable?	11
2.2.3	Magnetic Cataclysmic Variables	12
2.2.4	Flickering and Rapid Oscillations	13
2.2.5	SDSS J0155	14
2.3	Rapid Variability in X-ray Binaries	16
2.3.1	System Parameters and Geometry	16
2.3.2	QPOs in X-ray Binaries	18
2.3.3	QPO Model for Low-Mass X-ray Binaries	18
2.3.4	QPO Model for Black-Hole Binaries	18
2.3.5	The Black-Hole Binary Cygnus X-1	20
3	Photon-Stream Properties and Instrumentation for Their Study	22
3.1	Introduction	22
3.2	Photon Statistics	22
3.2.1	Fourier Transforms	22
3.3	Instrumentation	24
3.3.1	OPTIMA–Optical Pulsar TIMing Analyser	24
3.3.2	QVANTOS–Quantum Optical Spectrometer	26
3.3.3	Flex 01-05D and Development of the Software Program PhoCorr	26
4	Applications of High-Speed Astrophysics	30
4.1	Introduction	30
4.1.1	Skinakas Observatory	31
4.2	Preparations for the Observing Campaign	31
4.3	Observing Campaign at Skinakas Observatory	33
4.3.1	Observed Sources	34
4.3.2	Observations of SDSS J0155	35
4.3.3	Observations of Cygnus X-1	35

4.4	Data Analysis	36
4.4.1	SDSS J0155, Analysis of Observations	37
4.4.2	Cygnus X-1 and Telescope Vibrations	41
5	Summary and Possible Future Projects in High-Speed Astrophysics	53
5.1	Summary	53
5.2	Future Projects	54
A	Programs	58
A.1	Light Curves	58
A.2	Power Spectra	58
A.2.1	SigmaPlot	58
A.2.2	MATLAB	58
B	Manual and User Guide for the Digital Correlator <i>Flex01-05D</i> and the Control-Program <i>PhoCorr</i>	62
B.1	Introduction	62
B.2	Basic correlator specifications	62
B.2.1	Mode A: Single auto/cross correlation	62
B.2.2	Mode B: Quad correlation	63
B.2.3	Mode C: Dual auto/cross correlation	63
B.2.4	Photon history recorder	63
B.2.5	Calculating the correlation functions	63
B.3	LabVIEW	64
B.4	Flexx01	64
B.4.1	USB Initialize	64
B.4.2	USB Start	65
B.4.3	USB Update	65
B.4.4	USB Stop	65
B.4.5	USB Free	65
B.5	PhoCorr	66
B.5.1	Interpreting the block diagram	66
B.5.2	How to use PhoCorr	67
B.6	Appendix	69

Abstract

Quasi-periodic oscillations (QPOs) are rapid phenomena observed in accreting binary systems such as *cataclysmic variables (CVs)*, *low-mass X-ray binaries (LMXB)*, and *black-hole candidate binaries (BHC-binaries)*. In these systems matter is transferred to the primary white dwarf, neutron star or black hole. The rapid oscillations are produced by the same physical mechanism in all systems, originating from the accretion region.

Measuring rapid oscillations requires high temporal resolution. With high resolution the data rates are very high and it is not practical to measure a light curve in a conventional way. A high-speed detector system could include some kind of photon counting detectors such as avalanche photo-diodes (APDs) connected with a *hardware correlator* that reduces the amount of data and makes it possible to show fast variability in real time.

The main goal of this diploma work was to explore optimal methods for observing rapid variability in compact objects. A major part of the work was to develop a control program for the correlator Flex 01-05D and to test its possibilities in actual astronomical observations.

In the first part of this diploma work a correlator purchased from the company "Correlator.com" was evaluated for later use during observations of sources with possible QPOs, and a control program was developed to display and store the data more easily. In the second part, the correlator was used with the high speed-detector system *OPTIMA*¹ during an observation campaign at the 1.3 m telescope at Skinakas Observatory on Crete. Measurements of different compact objects such as CVs, LMXBs, BHC-binaries and pulsars were obtained. Intensity traces and correlation functions were acquired and power spectra were later calculated and analyzed in particular for the cataclysmic variable *SDSS J0155* and the black-hole candidate *Cygnus X-1*. These objects were some of the chosen candidates in the search for measurable QPOs. Variabilities on short time-scales were present in both sources and whether these arose from QPOs or not were investigated.

Key words: Cataclysmic Variables, SDSS J0155–X-Ray Binaries–Black-Hole Binaries, Cygnus X-1–QPO–High-Speed Astrophysics–Hardware Correlator

¹The OPTIMA system is developed by a group at the Max-Planck Institute for Extraterrestrial Physics (MPE) in Garching near Munich.

Sammanfattning

Kvasiperiodiska oscillationer (QPOs) är snabba intensitetsfluktuationer som kan observeras i kompakta dubbelsystem såsom *kataklysmiska variabler*, *röntgendubbelstjärnor* samt *svarta-håls dubbelstjärnor*. I dessa system strömmar materia från den ena stjärnan till det kompakta objektet som kan vara en vit dvärg, neutron stjärna eller ett svart hål. Intensitetsfluktuationer kan skapas i denna process och kan observeras som QPOs.

För att kunna mäta snabba förlopp i dessa system behövs hög tidsupplösning men detta kan skapa mycket stora datamängder och dessa måste därför reduceras för att kunna hanteras. Ett sätt att reducera datamängden är att använda *korrelatorer*. Ett system för att mäta snabba förlopp på kompakta objekt skulle exempelvis kunna bestå av fotonräknande detektorer såsom lavindioler sammankopplade med korrelatorer som reducerar den inkommande datamängden och kan visa eventuella periodiciteter i ljuskällan.

Syftet med detta examensarbete var att finna optimala metoder för att kunna observera snabba förlopp kring kompakta objekt. En stor del av arbetet gick ut på att utveckla ett mjukvaruprogram till korrelatorn samt att testa denna i observationer av kompakta objekt.

I den första delen av examensarbetet utvärderades en korrelator som tillhandahållits från företaget "Correlator.com". Denna skulle senare användas vid observationer av system, eventuellt uppvisande QPOs. Ett mjukvaruprogram utvecklades även för att kunna spara och lättare visa inkommande mätdata. Vi fick i andra delen av examensarbetet möjlighet att testa korrelatorn och dess program vid observationer av några kompakta objekt med ett 1,3-meters teleskop vid Skinakas observatoriet på Kreta i oktober 2004. Korrelatorn var sammankopplad med detektorsystemet *OPTIMA*² och observationer av kompakta objekt såsom kataklysmiska variabler, röntgen dubbelstjärnor, svarta håls kandidater och en pulsar genomfördes. Två av huvudobjekten som observerades var den kataklysmiska variabeln *SDSS J0155* och svarta-hål dubbelstjärnan, *Cygnus X-1*. Vi fann periodiciteter i båda objekten och analyser gjordes för att utröna om dessa kom ifrån objektet självt.

Nyckelord: Kataklysmiska variabler, SDSS J0155–Röntgendubbelstjärnor–Svarta-håls dubbelstjärnor, Cygnus X-1–QPO–Höghastighets-astrofysik–Korrelator

²OPTIMA är utvecklat av en grupp vid Max-Planck Institutet för Extraterrest Fysik (MPE) i Garching nära München.

Chapter 1

Introduction

1.1 What is High-Speed Astrophysics? (HSA)

New discoveries in astronomy are often made when technology is improved. Most wavelength regions are nowadays accessible and new technology makes it possible to reach for even higher spatial and temporal resolution. With the temporal resolution that can be achieved today it is possible to detect high-speed phenomena on time scales of seconds, milliseconds and maybe microseconds that exist in different kinds of objects. On shorter time scales, it may even be possible to detect quantum effects.

Different phenomena that occur in various wavelength regions and time scales are illustrated in *figure 1.1 and 1.2*. The time scale is plotted versus electromagnetic wavelength. All regions are not accessible at the present time due to e.g. insufficient observable photon flux.

1.2 Where are High-Speed Phenomena Present?

High-speed phenomena are expected to be present in sources and processes as;

- Instabilities in accretion discs around compact objects.
- Radial oscillations in white dwarfs ($\sim 100\text{--}1000$ ms) and non-radial oscillations in neutron stars (≥ 100 μs).
- Instabilities in the accretion flow onto white dwarfs and neutron stars (Plasma instabilities and fine structure).
- Optical emission from millisecond pulsars (≥ 10 ms).
- Fine structure in the emission from pulsars and other compact objects (Photon showers).
- Photo-hydrodynamic turbulence in extremely luminous stars (Photon bubbles).
- Stimulated emission from magnetic objects (Cosmic free electron laser).

Several studies of these phenomena have been conducted in the optical and X-ray region. One would think that the X-ray region would be ideal for short time-scale observations since X-rays often are emitted from hot regions close to the compact objects where the high-speed phenomena exist. However, the number of detectable photons with foreseeable instruments is

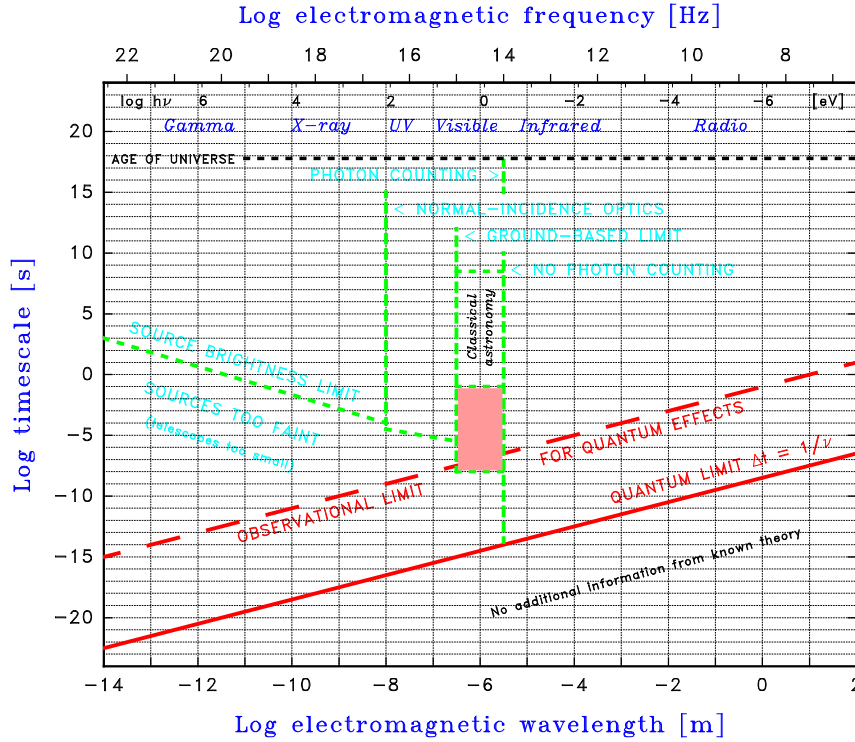


Figure 1.1: *Different phenomena that occur in various wavelength regions and time scales are shown. Time scale is plotted versus electromagnetic wavelength (Dravins, 1994).*

much greater from the optical region and this area is therefore much better suited for short time-scale observations.

The focus in this thesis will be on rapid phenomena close to compact objects in binary systems. This involves quasi-periodic oscillations (QPOs) created in the accretion flow onto white dwarfs in cataclysmic variables (CVs) and in the inner parts of the accretion disc in X-ray binaries (XRBs), close to the central neutron star or black hole.

1.3 How Can these Rapid Phenomena be Detected?

The phenomena studied in this thesis take place in the region of seconds and possibly milliseconds. At high temporal resolution, the data rates are very high and there is a need for statistical presentation of the incoming photon stream. Correlation functions can be used to find periodicities in the intensity data. The correlation function is proportional to the square of the intensity and this makes larger telescopes more sensitive to high-time measurements than smaller ones. Therefore, large optical telescopes facilitate the observations of fast variabilities. There is a need for real-time reduction of the incoming photons to be able to handle the data. One would also like to measure variability shorter than the interval between successive photons for faint sources. This is not possible with a light curve, but with a correlation function containing statistics of the arrival times, the periodicities will be possible to distinguish.

Charge-coupled devices (CCD) have been the dominating detector type in the optical region because of their high quantum efficiency, but their relatively long readout times make them difficult to use for measuring rapid variability. Instead photocathode detectors such as photomultipliers have been used because they can time individual photons. However their limit in quantum efficiency and limit in the extension towards infrared have led to a need for new types of detectors. An ideal high-speed detector should have high quantum efficiency to be able to detect

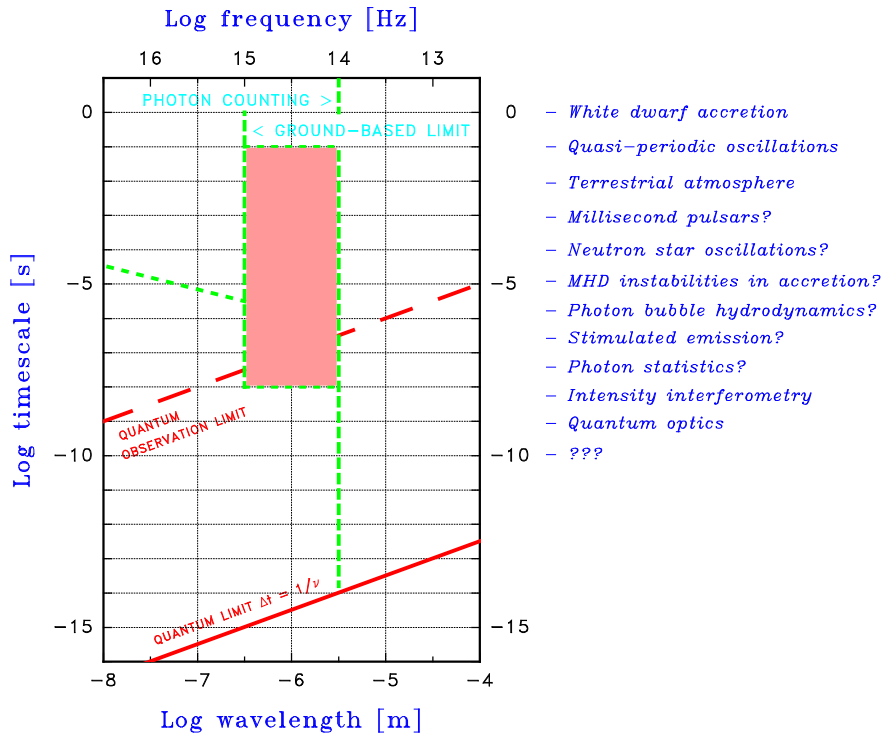


Figure 1.2: A region from 10 nm–100 μ m is shown, with expected time scales for various astrophysical processes marked (Dravins, 1994).

photons from weak sources and a time resolution of nanoseconds. They should be sensitive into the infrared region to be able to detect reddened sources and such with high redshift. Avalanche photo-diodes (APDs) are currently used for these kinds of observations. With their high quantum efficiency and fast readout times they are useful in high-speed astrophysics although their small dimensions can be a problem on large telescopes (*see Ch. 3*).

1.4 High-Speed Astrophysics at Lund Observatory

Lund Observatory has designed a unit to measure high-speed phenomena, QVANTOS (Quantum Optical Spectrometer). It was used on La Palma to explore the atmospheric scintillation on short time-scales. This was done to understand what kind of rapid variability that can be detected from the terrestrial atmosphere and that might be interfering with astronomical measurements (Dravins, 1997ab, 1998).

A new portable hardware correlator Flex01-05D from the company Correlator.com was purchased to Lund Observatory in 2002. In the first part of this diploma work, the correlator was evaluated and a control program was developed in the LabVIEW programming environment to make the presentation and storage of the incoming data adjusted for use in HSA. The second part of the diploma work was conducted in collaboration with the OPTIMA group at Max-Planck Institute for Extraterrestrial Physics in Garching. The compatibility between the correlator and their APD-detector system OPTIMA was tested during three days in Garching, June 2004. The two systems were found to be fully compatible and a decision was made to join the group in an observation campaign at Skinakas Observatory on Crete, Greece in October 2004. During the campaign, correlation functions and intensity traces were acquired for several compact systems likely to contain QPOs. Power spectra and correlation functions were later calculated and analyzed especially for the cataclysmic variable SDSS J0155 and the black-hole binary Cygnus X-1. These objects were some of the chosen candidates in the search for measurable QPOs. Variability

on short time scales was found to be present in both sources and whether these arose from QPOs or not was investigated.

The main goal of this diploma work was thus to explore and develop optimal methods for observing rapid variability in compact objects. A major part of the work involved developing a control program for the correlator Flex 01-05D and testing its possibilities in actual astronomical observations of such sources.

Chapter 2

Astrophysical Challenges

2.1 Introduction

Phenomena on short time scales are observed in compact binary systems. *Cataclysmic variables (CVs)* are low-mass members of the objects called *interactive binaries* and include subclasses such as *novae*, *dwarf novae* and *nova likes*. The main-sequence secondary star, a red dwarf is transferring matter onto the primary, a white dwarf. Intensity variations in form of *quasi-periodic oscillations (QPOs)* on short time scales occur in the accretion region. In some CVs, the magnetic field of the primary is strong enough to prevent the formation of an accretion disc. Matter is then forced to move along the field lines directly onto the magnetic poles of the white dwarf. Shocks are created in this region which causes variability on the time scale of a few seconds or less. AM Her was the first discovered magnetic CV and is the prototype of these systems that are also called polars. The cataclysmic variable *SDSS J0155* studied in this thesis is of AM Her type.

Many of the rapid phenomena that occur in CVs are also present in *X-ray binaries (XRBs)*. These are systems with a primary of the type neutron star or black hole. The black-hole binary *Cygnus X-1* is one of the main objects studied in this thesis. Hot clumps orbiting the primary star can be seen as QPOs on time scales of milliseconds. Neutron stars having a low magnetic field can reach spin periods of milliseconds and QPOs are detected on these time scales. The quasi-periodic oscillations seen in X-ray binaries are very much alike the oscillations seen in the CV type called dwarf nova (Warner, 2004). Similarities between the rapid oscillations in CVs and XRBs indicate that they might have the same origin. It is found that 90 % of the energy in a compact system with a size of 10 km will be released within a radius of $\sim 10^2$ km. An ordinary disc has a radius of $\sim 10^{5-7}$ km depending on the distance between the binaries (Van der Klis, 2000). It is likely that the inner parts of the accretion region are turbulent and can create rapid intensity variations such as QPOs. In most models to describe XRBs, a Keplerian accretion disc is present down to a certain radius close to the compact object. Within this radius the matter is no longer moving in circular orbits but is spiralling down onto the primary star. The twin kilohertz quasi-periodic oscillation was one of the first millisecond phenomena found in XRBs. It was interpreted to originate from the orbital motion of the inner accretion flow.

It is an astrophysical challenge to observe rapid variability and to understand what is causing it. The quasi-periodic oscillations are not present all the time and can therefore be difficult to observe, but the study of them will contribute to a greater understanding of the nature of all compact binary systems.

2.1.1 What is a Quasi-Periodic Oscillation?

A QPO can be seen in the power spectrum as a Lorentzian peak that is characterized by its frequency, ν_{QPO} , its width, λ , and its strength. A QPO can be expressed in terms of a so called "quality factor", $Q = \nu_{QPO}/\lambda$. A peak must have a $Q > 2$ to be defined as a QPO (Van der Klis, 2000).

The QPOs will in this thesis be referred to as peaks in a correlation function or a power spectrum that can clearly be distinguished from the noise level. A peak of low amplitude that is barely distinguished from the noise level can be of interest if it can be detected in many data sets.

2.2 Cataclysmic Variables and their Rapid Phenomena

2.2.1 The Search for High-Speed Events in Cataclysmic Variables

Periodic oscillations in cataclysmic variables were found for the first time in the middle of the nineteenth century when N. Pogson found oscillations on time scales of 6-15 s in the nova U Gem. Because of the stable neighbouring stars he concluded that the variability must originate from the star itself. A. D. Thackeray observed VV Pup in the beginning of the 1950's. The star seemed to vary faster than was possible to detect photographically and visual observations were made as well. Until photoelectric photometry confirmed the variability seen in U Gem and VV Pup, nobody could be absolutely sure of their existence (Warner, 1988).

A method to extract more information from the light curves was used by Zuckermann in the beginning of the sixties. He examined the light curves of SS Cyg by digitizing them by hand and then tabulating the intensity for every 30 s. This was then evaluated by a computer and Fourier transforms were calculated. He found a periodicity of 16 min in the light-curve data and similar techniques were used on other cataclysmic variables (Warner, 1988).

It was difficult to continue the work because of the slow development of necessary technology but a rescue came in the late 1966. A fast digital counter was needed for the purpose of measuring atomic transition probabilities at Princeton University. The digital counter was linked to a pulse-counting UBV photometer on a reflector at the observatory at Princeton. This was the first digital recording device to be used in high-speed astronomical photometry (Warner, 1988).

Periodicities were found during the outburst of some cataclysmic variables and two types of oscillations were classified, DNO, dwarf novae oscillations, which had a high degree of coherence that lasted for about 100 cycles, and QPO, quasi periodic oscillations, which had coherence times as short as a few cycles. It was showed in the beginning of the eighties that a radiating accretion flow onto a white dwarf could undergo thermal instabilities which would produce brightness fluctuations on time scales of seconds (Warner, 1988).

2.2.2 What is a Cataclysmic Variable?

It is not possible to resolve binaries as close as CVs with available telescopes including the Hubble Space Telescope and the data from both components must be analyzed from light curves and/or statistical analysis of the incoming photon-stream. Eclipsed systems give the best opportunity for observations and systems with high inclination, $> 74^\circ$ will be observed as totally or partially eclipsed systems (Wiehahn et al., 2004). The short time it takes for the eclipsed star to enter or leave the eclipse indicates that it is tiny. We know the speed of the eclipsing star by its orbital period and then how far it has moved in the time it takes for it to become completely eclipsed and this gives the size of the eclipsed star. The eclipsed star in CVs is of the size of earth and must therefore be a white dwarf which has a mass limited by the Chandrasekhar limit ($\approx 1.4 M_\odot$). The mass-losing red dwarf has an typical radius and mass of $\approx 0.15 R_\odot$ and $\approx 0.3\text{--}1.3 M_\odot$, respectively, where $R_\odot = 6.960 \cdot 10^8$ m and $M_\odot = 1.989 \cdot 10^{30}$ kg (Hellier, 2001).

Roche Geometry and Mass Transfer

Roche-lobe geometry is used to describe the interaction between the stars in binary systems. The inner Lagrangian point, L_1 is the apex of the Roche lobe. Assuming circular orbits because of tidal forces and that the centre of mass of each star is at the star's centre, the Roche geometry can be simplified to a usable expression. The gravitational potential ϕ at a point specified by the vector \bar{r} (the sum of the potentials of the two stars) can be expressed as in *equation 2.1* where M_1 , M_2 are the masses located at r_1 , r_2 and ω is the angular frequency of the orbit. G is the gravitational constant, $6.672 \cdot 10^{-11}$ N m²/kg².

$$\phi = -\frac{GM_1}{|r - r_1|} - \frac{GM_2}{|r - r_2|} - \frac{1}{2}(\omega \times \bar{r})^2 \quad (2.1)$$

Different consequences when varying ϕ can be studied in *Figure 2.1*. When ϕ increases, the stars first touch and then merge together (Hellier, 2001). The Roche geometry is specified by the mass ratio $q = M_2/M_1$ and the separation a between the stars. All cataclysmic variables are semi-detached. A secondary star that fills its Roche lobe emerges a thin stream of material at the speed of sound, ≈ 10 km/s from the Lagrangian point. In the case of a non-magnetic or low-magnetic CV, the Lagrangian point moves perpendicular to the stream at the speed of 100 km/s. This will force the material to flow into a disc surrounding the white dwarf. The material settles down into the orbit with the lowest energy at the "circularization radius". Material closer to the primary will orbit faster and the friction will make the material spread out into a thin disc. The inner edge will hit the white dwarf and matter will begin to spiral down to it while in the outer edge of the disc, the red dwarf will soak up angular momentum and draw material back to it. The stream from the secondary hits the accretion disc in a point called the "bright spot". Oscillations are expected from this region and from the inner parts of the accretion flow.

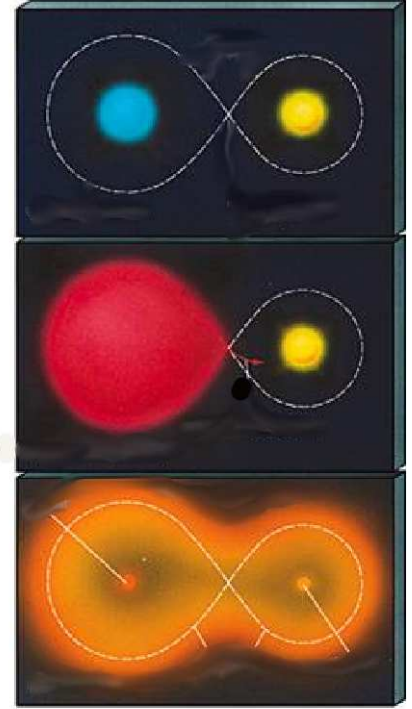


Figure 2.1: *Top: A detached binary. Middle: A semi-detached binary where matter is transferred from the secondary star. Bottom: A contact-binary where both stars overflow their Roche-lobe* (<http://www.astro.psu.edu/users/rbc/a1/Lec16.ppt>).

The white dwarf spins at a speed of about 300 km/s, but just above the surface, the Keplerian velocities of the accreting material is about 3000 km/s. Material needs to be slowed down before it can enter the white dwarf. Kinetic energy is converted to heat and is radiated away and this so called "boundary layer" can emit up to half of the total luminosity of the system.

2.2.3 Magnetic Cataclysmic Variables

AM Her was the first cataclysmic variable found to have a strong magnetic field and it became the prototype for the group known as polars (Warner, 1988). My personal vision of an accreting polar can be seen on the title page. In polars, the magnetic field is strong enough to produce synchronous rotation and the gas from the secondary becomes ionized and flows along the field lines onto the magnetic polar caps of the white dwarf. Inside the magnetosphere, the matter is locked to the field lines and then to the rotation of the white dwarf. The spin period of the white dwarf is adjusted so that the spin period inside the magnetosphere is equal to the spin period just outside the magnetosphere. Matter is forced to follow the field lines already from the Lagrangian point and the stream is then divided into two parts, one heading for the north magnetic pole and one for the south. The stream is concentrated in a tiny accretion spot near the pole and the matter hits the white dwarf at nearly free fall at a speed of 3000 km/s. Due to the impact, a column that will reduce the velocity of the incoming stream, rises above the surface of the white dwarf. Shocks are created in the impact area and kinetic energy is converted into X-rays by the bremsstrahlung process and is then radiated away. The area around the column has a temperature of 200,000 K (Warner, 1988). Matter breaks up into dense blobs in the region where the stream is first affected by the magnetic field and these blobs can oscillate up and down the column and be observed as QPOs.

Cyclotron Emission

The electric field in un-polarized light is pointing in every direction that is perpendicular to the direction of travel. Charged particles spiral around the field lines and any current moving perpendicular to the field lines will experience a force that makes the charged particles move in a circle due to the Lorentz force, $F = e(\vec{E} + \vec{v} \times \vec{B})$, where e is the electron charge ($-1.602 \cdot 10^{-19}$ As), v is the velocity of the particle, E and B is the strength of the electric respectively the magnetic field. A charged particle will have one motion along the field line and one around it and this result in a spiralling motion and polarized light (Figure 2.2). The circular motion gives acceleration to the particles and photons are emitted. The cyclotron radiation is about half of the total light of a polar and this makes them the most polarized objects in the sky. Studying the cyclotron emission from a polar can give information about the magnetic-field strength of the system.

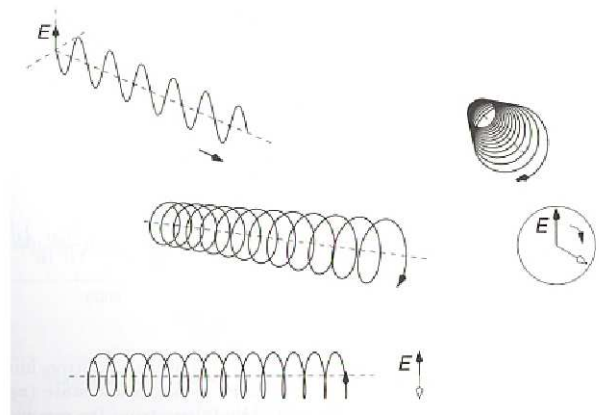


Figure 2.2: *Top left; an electric vector of a photon is perpendicular to its motion. Bottom; linearly polarized photons are produced when the field line is observed on the side, this produces an "up and down" motion. Right; circularly polarized photons are seen in the line of sight (Hellier, 2001).*

2.2.4 Flickering and Rapid Oscillations

There are several parts within the CV-system that can cause rapid variations. The white dwarf itself can oscillate and cause QPOs. The frequency depends on the density of the star. Small, dense stars have typical periods of a few 100 s. Flickering is variations referred to as red noise (white noise has equal amplitudes at all frequencies but this is not the case for red noise). Red noise is expected from a turbulent flow such as an accretion stream. The flickering is reduced in a system when the disc and bright spot is eclipsed, indicating that this might be its origin. Dwarf Nova Oscillations and Quasi Periodic Oscillations are phenomena seen as rapid brightness modulations on different time scales. The phenomena seem to be caused by the influence of a magnetic field and originate from the inner accretion region. A period-luminosity relationship exists that shows a relationship between the DNO-period and its optical brightness. Different types of oscillations can be present within the same system which means that oscillations can be created in different regions (Warner, 2004). *Figure 2.3* shows a Fourier spectrum of the cataclysmic variable TY PsA. A QPO, lpDNO and DNO is present in the same spectrum.

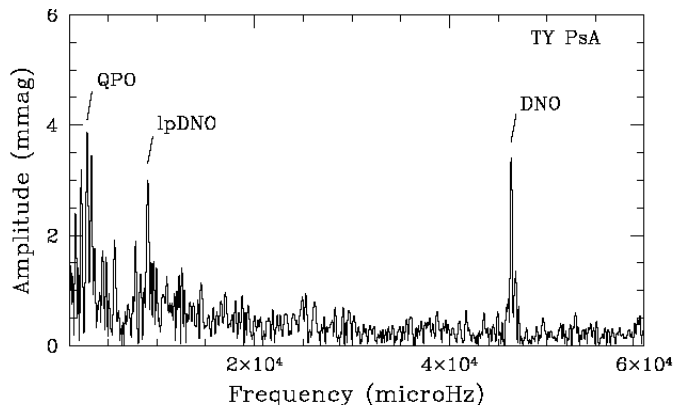


Figure 2.3: *Fourier spectrum of TY PsA where a QPO (Quasi Periodic Oscillation), lpDNO (longer period Dwarf Nova Oscillation) and an DNO (Dwarf Nova Oscillation) is present at the same time (Warner, 2004).*

QPOs are seen on different time scales and are modulations with less coherence than DNOs and can therefore be more difficult to detect. QPOs of a few seconds or less have been observed in polars and this is the type of oscillation studied in this thesis. These types of QPOs that are usually observed in polars have also been observed in dwarf novae outburst. Models such as the "Low Inertia Magnetic Accretor model" (LIMA) presented by Warner (2004) have been created to explain the origin of these QPOs. Matter is accreting through the disc onto the surface of the white dwarf and a rapid rotating belt around the equator of the white dwarf is formed as a result of the accretion. This will enhance the magnetic field of the white dwarf and can make it strong enough to make the material channel directly onto the equatorial belt (but not onto the magnetic poles as in the case for polars). CVs that are called non-magnetic must have some influence of the magnetic field of the white dwarf to explain the observed QPOs. This means that QPOs on the time scale of a few seconds usually expected e.g. from polars can possibly be detected from other CVs as well.

QPOs are seen on different time scales and are modulations with less coherence than DNOs and can therefore be more difficult to detect. QPOs of a few seconds or less have been observed in polars and this is the type of oscillation studied in this thesis. These types of QPOs that are usually observed in polars have also been observed in dwarf novae outburst. Models such as the "Low Inertia Magnetic Accretor model" (LIMA) presented by Warner (2004) have been created to explain the origin of these QPOs. Matter is accreting through the disc onto the surface of the white dwarf and a rapid rotating belt around the equator of the white dwarf is formed as a result of the accretion. This will enhance the magnetic field of the white dwarf and can make it strong enough to make the material channel directly onto the equatorial belt (but not onto the magnetic poles as in the case for polars). CVs that are called non-magnetic must have some influence of the magnetic field of the white dwarf to explain the observed QPOs. This means that QPOs on the time scale of a few seconds usually expected e.g. from polars can possibly be detected from other CVs as well.

Rapid Oscillations in Polars

QPOs of a few seconds have been discovered in some AM Her systems e.g. EF Eri and VV Pup (*figure 2.4*). These systems show an almost linear relationship between magnetic field strength and mean QPO frequency (Larsson, 1998). The QPOs are thought to originate from the shock column. During eclipses it might be possible to notice if the QPOs are located in different regions of the column and if there are several QPOs coexisting at different frequencies. QPOs can be absent for some time as seen in the system VV Pup. It is assumed that this might be due to

a decrease in the mass-transfer rate. Blobs of sizes about $1.5 \cdot 10^7$ m from the accretion stream will randomly fall into the accretion column and create perturbations. If the oscillations are dominated by one blob it can sometimes be seen directly in the light curve. It is more common that several blobs are acting independently with different phase and different periods (Hellier, 2001).

2.2.5 SDSS J0155

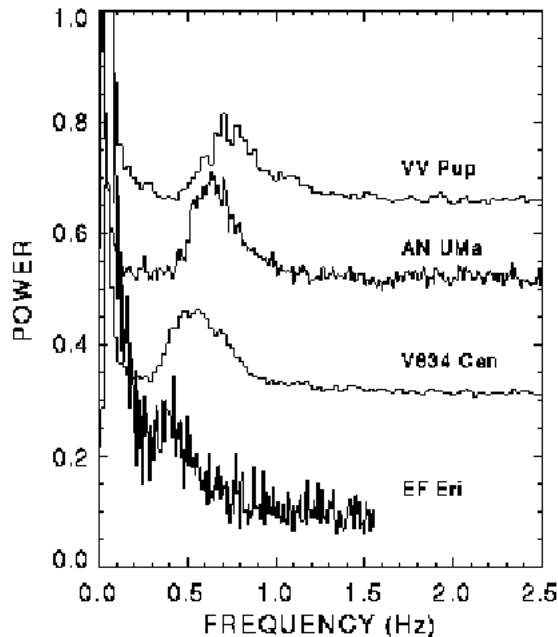


Figure 2.4: *Power spectra from optical high-speed photometry of four polars which has QPOs on the time scale of 1-3 s (Larsson, 1998).*

The eclipsing polar SDSS J0155 (SDSS J015543.40+002807.2) was first discovered in the *Sloan Digital Sky Survey* (SDSS) in Nov 2000 by Szkody et al. (2002). Photometric, polarimetric and spectroscopic measurements have been done during the last two years and the system shows large brightness variations. The orbital period of 87.13 minutes is the shortest period of any eclipsing polar known.

Szkody et al. (2002) observed SDSS J0155 in the year of 2000. Time-resolved data showed the system in a high brightness state and He II emission that usually is seen in accreting systems at λ 468.6 nm was evident. Because of the presence of *He II* and strong emission at the bright state Szkody et al. (2002) suggested SDSS J0155 to be an AM Her or an SW Sex Star¹. The orbital period of 87 min was arguing against an SW Sex system since they usually have longer orbital periods (Szkody et al., 2002).

After the first discovery, Dubkova et al. (2003), observed the system in 2002. Optical photometry of the system was obtained during high state ($m_V \approx 15.2$) and they found a deep and narrow eclipse superposed on a broad hump. (Figure 2.5) They interpreted this as a system with

¹SW Sextantis star has a definition based on spectroscopic properties and not photometric as other variable stars. A SW Sex system is a nova-like variable with a typical orbital period of 3-4 h (Taylor et al., 1999).

In the second part of this diploma work, the AM Her system SDSS J0155 was observed with the 1.3 m telescope at *Skinakas Observatory* on Crete in October 2004 (*Chapter 4*). As described above, oscillations of a few seconds have been observed from polars but no such variations have earlier been found in SDSS J0155. If the geometry is favourable, e.g. if the accretion column and the accretion stream can be detected for some part of the period, it is plausible to be able to detect rapid oscillations in this object.

Several observations of SDSS J0155 have been done during the past years and it is necessary to understand the geometry of the system to be able to identify the origin of possible oscillations. I will present some of the results of the observations and measurements made during the past years of SDSS J0155 to easier understand the results of the measurements obtained at Skinakas Observatory.

Observations During the Years 2000-2004

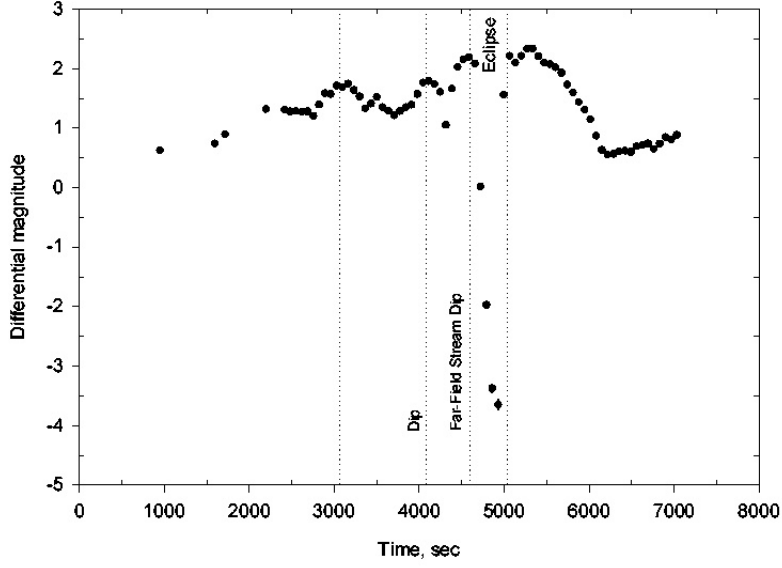


Figure 2.5: *V*-filter light curve of SDSS 0155. Zero-point of the time scale is JD2452506.6157 (Dubkova et al., 2003).

a dominating single accretion pole that is self eclipsed by the white dwarf for less than half of the orbit. The unusually deep minimum could be due to a total eclipse of the white dwarf and the accretion stream by the secondary.

Wiehahn et al. (2004) made photometric and polarimetric observations during the year 2003. The circular polarization plot shows both negative and positive polarizations and the negative part shows a double hump feature. (Figure 2.6) The change in the sign of the polarization can be interpreted as a two-pole accreting system. One other thing that could explain the change in sign is the case where a tall enough shock column is seen with the field lines facing away from the observer as the region disappears behind the limb of the primary. The circular polarization will reverse sign when studying the column from underneath (Wiehahn et al., 2004).

System Parameters

Wiehahn et al. (2004) use the relationships in the equations 2.2 and 2.3 to get the values $\frac{M_2}{M_\odot} = 0.07 \pm 0.03$ and $\frac{R_2}{R_\odot} = 0.13 \pm 0.06$.

$$\frac{M_2}{M_\odot} = (0.126 \pm 0.011)P_{orb}(h) - (0.11 \pm 0.04) \quad (2.2)$$

$$\frac{R_2}{R_\odot} = (0.117 \pm 0.004)P_{orb}(h) - (0.041 \pm 0.018) \quad (2.3)$$

Further system parameters were obtained by estimating the mass of the white dwarf. A mean value of the mass of the white dwarf in polars is $\frac{M_1}{M_\odot} = 0.80 \pm 1.14$, as quoted by Wiehahn et al. (2004). They use the mass range of $0.66 < \frac{M_1}{M_\odot} < 0.94$ which gives a mass ratio of $0.11 < q < 0.07$. The separation between the centres of mass of the binary components is given by the expression 2.4;

$$a = 3.53 \times 10^{10} \left(\frac{M_1}{M_\odot} \right)^{1/3} (1 + q)^{1/3} P_{orb}^{2/3}(h) \quad (2.4)$$

This gives a value between $(4.1 \pm 1.1) \times 10^{10} < a < (4.5 \pm 1.2) \times 10^{10}$ cm using the above mentioned mass range for M_1 . An inclination calculated from the eclipse width and the mass ratio q lies in the range between $85^\circ < i < 90^\circ$. An accretion column of height $\sim 0.01 R_1$ is assumed.

2.3 Rapid Variability in X-ray Binaries

The X-ray binary systems can be divided into subclasses as *LMXB*, *low-mass X-ray binaries* and *HMXB*, *high-mass X-ray binaries*. Matter from the secondary star is accreting onto a disc surrounding a primary star of type neutron star or black-hole. QPOs are expected from the inner part of the accretion disc. Rapid oscillations have been detected from X-ray binaries since a couple of decades. A 20 s oscillation was detected in the object Sco X-1 in the beginning of the seventies and this was the first object found to be a member of the subclass low-mass X-ray binaries (Warner, 1998). A model to explain the origin of the QPOs was presented in the middle of the eighties. It was suggested that the oscillations found in many X-ray binaries were caused by interaction between the rapidly spinning neutron star's magnetic field and the matter circulating in the accretion disc. It was also found that different QPO-frequencies can be present within the same source. The search for QPOs in X-ray binaries continued with the launch of the RXTE satellite² and it has been collecting data of neutron star X-ray binaries since 1995. It discovered the first accretion driven millisecond pulsar, SAX J1808.4-3658. It also discovered the twin quasi periodic oscillations that have been observed at frequencies between 300-1300 Hz in many X-ray binaries (Wijnands, 2000).

2.3.1 System Parameters and Geometry

LMXBs are different from HMXBs e.g. the emitted optical light from a LMXB is dominated by emission from the accretion disc (Van der Klis, 1989). The light from the visible region in HMXBs is dominated by the luminous secondary and QPOs from the accretion flow of the primary are difficult to detect. QPOs are instead seen that originate from the early-type secondary (Warner, 1998). LMXBs have a secondary mass-losing star of a mass of $\lesssim 1 M_\odot$ while the HMXBs have a secondary of mass $\gtrsim 10 M_\odot$. The magnetic field in HMXBs is disrupting the accretion flow far above the surface of the primary star ($\sim 10^6$ m) while the accretion flow in LMXBs can extend

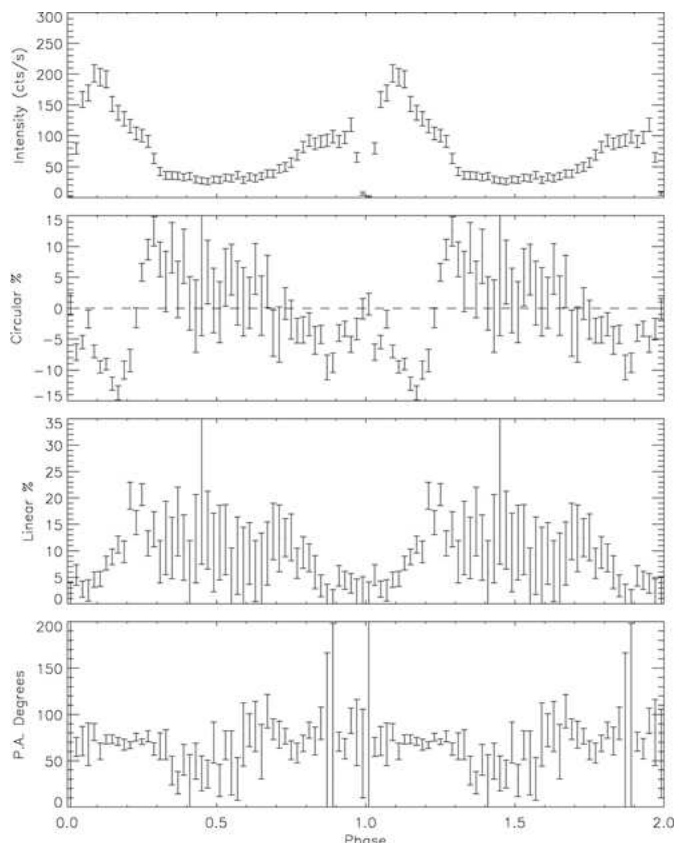


Figure 2.6: *Photometric and polarimetric data in white light (Wiehahn et al., 2004).*

²Rossi X-ray Timing Explorer (RXTE) was launched by NASA in December 1995. It observes objects as BHC, neutron stars, X-ray pulsars and X-ray bursts with high time resolution.

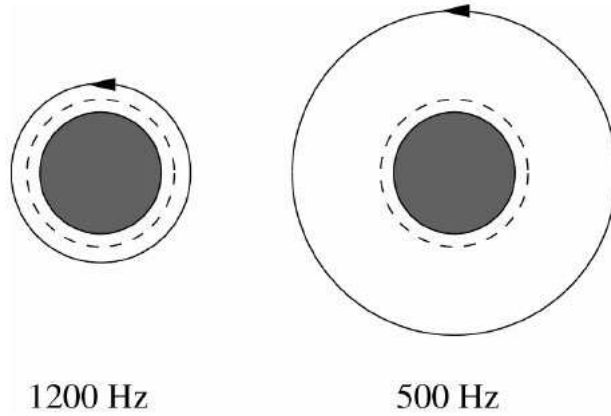


Figure 2.7: The innermost stable orbit is presented with a dashed line and has radius of 10 km. A $1.4 M_{\odot}$ neutron star is situated in the middle. QPOs are created at different frequencies depending on where in the accretion disc the clumps are situated (Van der Klis, 2000).

further down so that a radiation-pressure dominated accretion disc can exist. The radiation pressure forms a thick accretion region. Relativistic jets could form as observed in Sco X-1.

It is believed that a Keplerian accretion-disc is present down to a certain radius close to the primary, compact object in X-ray binaries. Within this radius the material is no longer moving in circular orbits but is spiralling down to the primary star. Characteristic velocities near the compact object are of the order $\frac{GM}{R}^{1/2} \sim 0.5 c$ and the timescale for the motion of matter through the emitting region is, $\tau = \frac{r^3}{GM}^{1/2} \sim 0.1$ ms for an radius of 10 km and ~ 2 ms for an radius of 100 km near a $1.4 M_{\odot}$ neutron star and ~ 1 ms at 100 km from a $10 M_{\odot}$ black hole. This indicates that millisecond is a natural time scale for accretion processes. The orbital motion around a neutron star occurs at a frequency described by *equation 2.5*, and at a orbital radius, as in *equation 2.6*, were $m_{1.4}$ is the stars mass in units of $1.4 M_{\odot}$. No stable orbital motion is possible within the innermost stable circular orbit (ISCO), $R_{ISCO} = 6 GM/c^2 \approx 12.5 m_{1.4}$ km. The frequency of orbital motion at the ISCO is approximately, $\nu_{ISCO} \approx (1580/m_{1.4})$ Hz. A Schwarzschild geometry and a non-rotation spherically symmetric neutron star or a black hole is assumed. *Figure 2.6* show the orbits of matter circulating around a neutron star of mass $1.4 M_{\odot}$ that are corresponding to the orbital frequencies of 1.2 and 0.5 kHz (Van der Klis, 2000).

$$\nu_{orb} = \left(\frac{GM}{4\pi^2 r_{orb}^3} \right)^{1/2} \approx 1200 Hz \left(\frac{r_{orb}}{15 km} \right)^{-3/2} m_{1.4}^{1/2} \quad (2.5)$$

$$r_{orb} = \left(\frac{GM}{4\pi^2 \nu_{orb}^2} \right)^{1/3} \approx 15 km \left(\frac{\nu_{orb}}{1200 Hz} \right)^{-2/3} m_{1.4}^{1/3} \quad (2.6)$$

Black-Hole Binaries

It is assumed that several X-ray sources in our galaxy are BHC-binaries where matter is accreting down onto a black hole. The strongest evidence for the existence of a black-hole binary is the measurement from optical observations that the companion star is orbiting a mass that is larger than $3 M_{\odot}$ which is the "Oppenheimer-Volkoff" limit. The light curve of a black-hole binary system is often chaotic and its spectrum fits an accretion model onto a body with no hard surface. (The opposite is found for neutron stars) Both LMXBs and HMXBs can contain a primary black hole. BHCs have a number of different X-ray intensity states. In low state the

mass-transfer rate, \dot{M} is low and the spectra hard. In the high state the \dot{M} is higher and the spectrum softer. Many black-hole binaries are difficult to study optically because of their position near the galactic plane or near the galactic center. A black hole can be described by its mass m , its angular momentum a and the electric charge contained within the event horizon. A Schwarzschild black hole is assumed to be uncharged. The event horizon is situated at the radius, $R_s = 2Gm/c^2 = 3m/M_\odot$ km. The accretion disc is containing stable orbits down to a radius $r > 3R_s$ and material at this radius has an orbital period of $P = 0.6 m/M_\odot$ ms. The radius $r = 3 R_s$ is the innermost stable orbit closest to the event horizon. (Dolan, 2001).

2.3.2 QPOs in X-ray Binaries

QPOs are detected from the accretion region in X-ray binaries and especially from the innermost stable orbit of the accretion disc. QPOs in X-ray binaries are defined to have a peak width of roughly half the QPO-frequency and amplitudes between 1 and 10 percent of the total frequency (Van der Klis, 1989). A relation between the frequencies of the QPOs and the accretion rate onto the primary has been confirmed by observations. Sources in strong gravity such as X-ray binaries show pairs of higher frequency QPOs with the higher frequency about 50 % larger than the lower frequency. The twin kilohertz oscillations can reach values as 1.2 kHz for neutron stars and 0.5 kHz for black holes. Twin kilohertz oscillations have not been observed in sources of Newtonian gravity (Bursa et al., 2004). However, the same sort of mechanism seems to be behind the QPOs observed in all types of compact binary systems and one of the common features is an accretion region.

2.3.3 QPO Model for Low-Mass X-ray Binaries

Models have been developed to understand the origin of the QPOs. Oscillations are assumed to be present e.g. when illuminated blobs near or in the innermost stable orbit are orbiting the primary star. The blob will be visible once per orbit and a periodic signal can then be detected. Other models describe rapid phenomena that are suspected to originate from a layer in the atmosphere of the primary star that rotates in near co-rotation with the neutron star itself. (Van der Klis, 2000)

Miller et al., (1996, 1998) (as quoted by Van der Klis, 2000) presents the *Sonic-Point Beat-Frequency Model* that is a modification of the *Beat-Frequency Models* developed by e.g. Alpar and Shaham, (1985). Material is orbiting in the disc at a radius r_{sonic} near the r_{ISCO} . At this radius the radial inflow velocity becomes supersonic. At r_{sonic} , clumps are accreting onto the neutron star in fixed spiral-shaped trajectories. The clumps are hitting the neutron-star surface at a certain region that becomes illuminated and can be observed as a hot spot moving around the surface at a speed corresponding to the orbital velocity of the clumps at r_{sonic} . This will produce an upper kilohertz oscillation at frequency ν_2 . The incoming clumps are of approximately the same size and have a lifetime of about 0.01–0.1 s. X-rays are generated by the accretion onto the magnetic poles and this beam is illuminating the clumps at the radius r_{sonic} once per beat period. This is modulating the rate of the incoming clumps and hence the emission from the hot spot of the neutron star surface. The lower kilohertz oscillation is created by this mechanism at frequency ν_1 . The Sonic-Point Beat-Frequency Model is illustrated in *figure 2.8*.

2.3.4 QPO Model for Black-Hole Binaries

In most QPO models for black-hole binaries, the QPO frequency corresponds to a characteristic frequency not very far from the inner edge of a Keplerian disc.

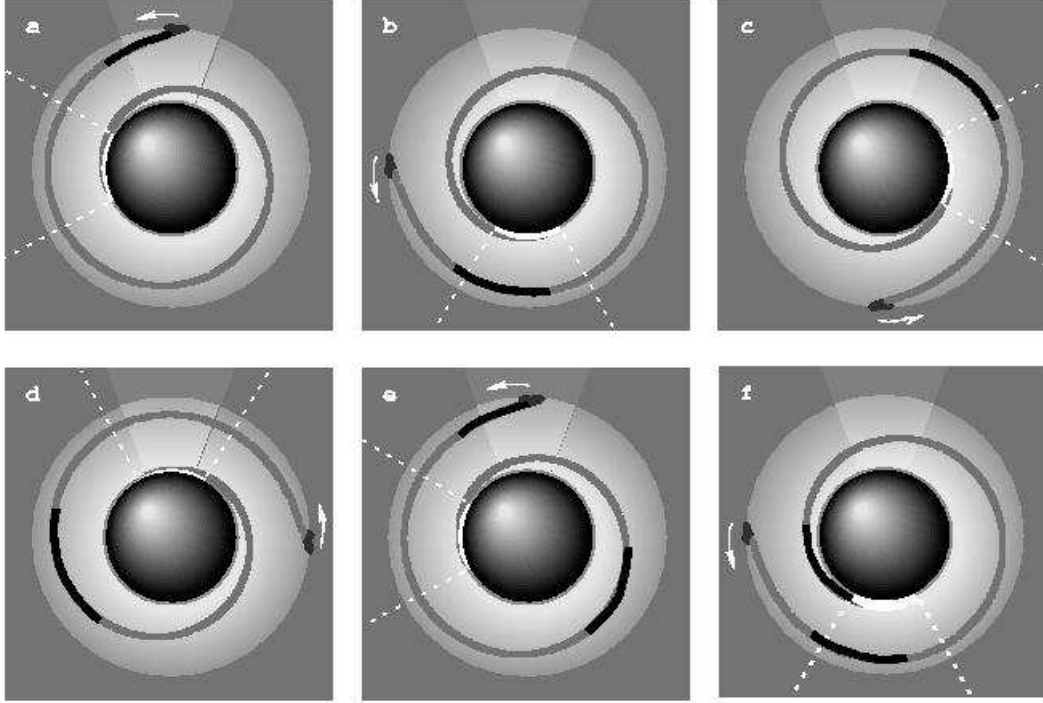


Figure 2.8: *In the Sonic-Point Beat-Frequency Model to explain QPOs in LMXBs, clumps are spiralling down onto the neutron star. The emission from the region where the clumps hit the white dwarf is seen as dashed lines. The clumps are illuminated by the beam from the magnetic pole of the neutron star at the radius r_{sonic} and they can be observed as QPOs (Miller et al., 1996, 1998 as quoted by Van der Klis, 2000).*

Bursa et al. (2004) show that an accretion disc in forms of a luminous torus, accreting around a Schwarzschild black hole, will create periodic variations even if the source of radiation is steady. QPOs will be created as the torus is oscillating up and down along the axis that is parallel to the symmetry axis and this oscillation can be observable in the inner accretion region near the compact object. A luminous, optically thin torus around the equatorial plane of a non-rotating black hole with a mass of $10 M_{\odot}$ is assumed. Near the black hole, gravitational lensing of the photon trajectories can modulate the flux received at infinity and this can be observed as QPOs. *Figure 2.9* shows the result of the numerical ray-tracing computations made by Bursa et al. (2004) for different viewing angles i of the system (from left; $i = 45^{\circ}, 65^{\circ}, 85^{\circ}$). Twin kilohertz oscillations at ≈ 0.1 kHz, are clearly seen in the power spectrum for all viewing angles. The lower peak is due to a change in the luminosity of the system but the upper peak is present due to relativistic effects caused by the strong gravitational field. The simulations show that twin kilohertz QPOs will be present in the power spectrum from light emitted from such a strong gravity source as a black hole. This can be compared with the results seen from sources in

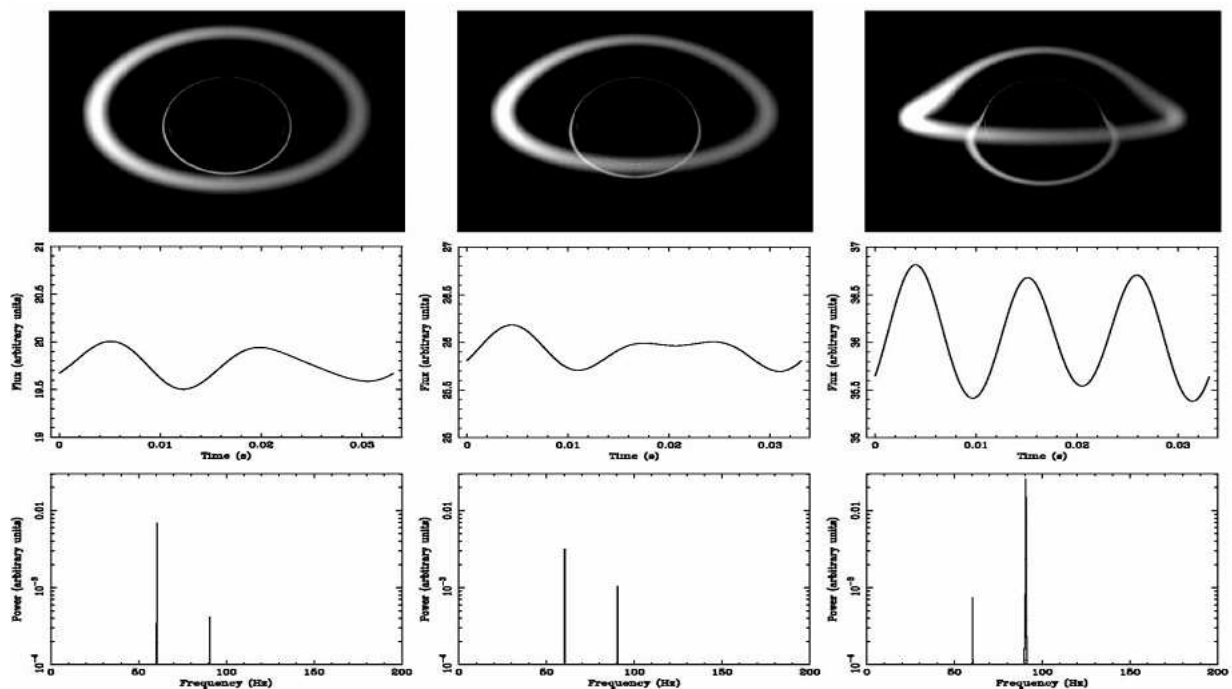


Figure 2.9: Numerical ray-tracing computations for a system with a luminous torus around a Schwarzschild black hole are shown for three different viewing angles. A twin kHz oscillation can be seen at approximately 0.1 kHz for all viewing angles (Bursa et al., 2004).

Newtonian gravity were only one oscillation is seen. This is in agreement with results presented by Abramowicz et al. (2003), who show that twin kilohertz oscillations can be created from a luminous torus surrounding a black-hole containing simultaneous oscillations in the radial and vertical directions at frequencies ω_r and $\omega_\theta = (3/2) \omega_r$. Both frequencies will show up in a power spectrum. In Newtonian gravity is $\omega_\theta = \omega_r$.

2.3.5 The Black-Hole Binary Cygnus X-1

Cygnus X-1 was the first compact object to be classified as a black-hole candidate and is one of the brightest X-ray sources in the sky. It is an HMXB which has a mass exceeding $6 M_\odot$. Its secondary star, HDE 226868, is a super giant of type O9.7Iab and the two stars are orbiting each other with a period of 5.6 days. The disc surrounding the black hole has a mass of several M_\odot . Cygnus X-1 is spending most of its time in its low state.

Periodic oscillations have been detected in Cygnus X-1 since 1974 and have been measured in different wavelength regions (Chaput et al., 2000). Variability on different timescales from years to milliseconds has been observed during both hard and soft state (e.g. the discovery of millisecond flares by Gierlinski et al., 2003, in both hard and soft state). Another temporal variation is the intensity dips that can be observed on timescales from minutes to hours. Chaput et al., (2000) have analysed data from observations of Cygnus X-1 performed by *HEAO A-1* (*High Energy Astronomical Observatory, A-1 experiment*) on May 7, 1978. Cygnus X-1 was in a low (hard) state during the observations. *Figure 2.10* shows a millisecond oscillation in the X-ray power-spectrum of Cygnus X-1 found using the HEAO A-1 data.

In this diploma work, observations of Cygnus X-1 were performed during an observing campaign at Skinakas Observatory, October 2004 (*chapter 4*).

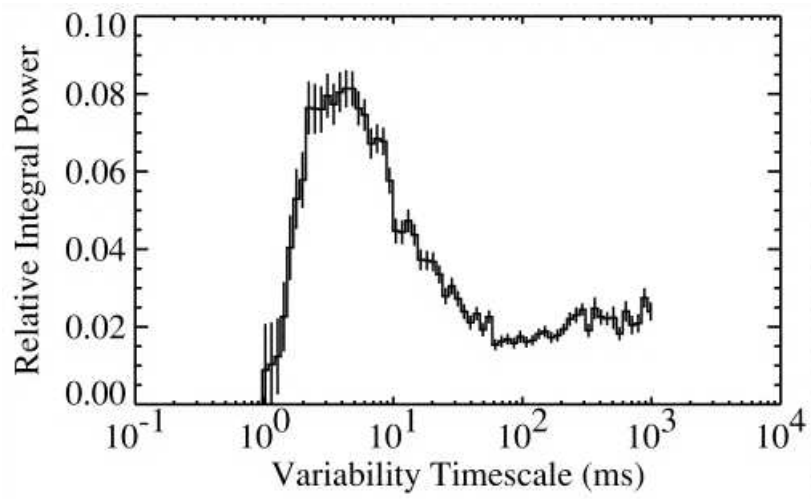


Figure 2.10: *A millisecond peak in the X-ray power-spectrum of Cygnus X-1 (Chaput et al., 2000).*

Chapter 3

Photon-Stream Properties and Instrumentation for Their Study

3.1 Introduction

The variability in the objects studied in this thesis is on time scales of seconds and possibly milliseconds. At high time resolution the data rates are high and there is a need for statistical presentation of the incoming photon stream. The photon noise varies as the square root of the number of photons detected. For faint stars this means that the noise in a high-time resolution light curve will be dominated by photon noise and that the time interval between incoming photons sometimes is larger than the searched time variability. Statistical analysis of the arrival times of the photons can reveal periodicities on time scales shorter than the time interval between successive photons. A reduction of the data in real time is necessary to handle the huge amount of incoming data while studying the shortest time scales. This can be done by a statistical presentation of the photon stream, e.g. correlation functions and power spectra. Instruments for use in high-speed astrophysics must have high quantum efficiency over a large wavelength range. A high-speed detector system could include some sort of photon-counting detectors such as APDs, which have a high time resolution and hardware correlators which reduce the incoming amount of data and display the variability on short time-scales.

3.2 Photon Statistics

3.2.1 Fourier Transforms

A light curve can be reproduced by summing a set of sine waves. The shortest variability that can be detected depends on the sample time of the light curve and frequencies faster than the *Nyquist frequency* can not be detected. The amplitude of each sine wave reveals how much of each frequency is represented and a Fourier transform is then produced by plotting the amplitudes against frequency. A light curve consists of N bins (N is assumed to be an even number). Each bin has a duration of τ and the j th bin contains n_j detected photons. The discrete Fourier transform $[\tilde{n}_j]$ of a set $[n_j]$ is described by the *equations 3.1, 3.2 and 3.3* (Warner, 1988).

$$[\tilde{n}_j] = [A_k] + i[B_k] \quad (3.1)$$

$$A_k = \frac{1}{N} \sum_{j=0}^{N-1} n_j \cos(2\pi k j / N) \quad (3.2)$$

$$B_k = \frac{1}{N} \sum_{j=0}^{N-1} n_j \sin(2\pi k j / N) \quad (3.3)$$

With the normalization $\frac{1}{N}$ a periodic signal in the data remains constant in the power spectrum and the noise decreases when N increases. Some use $(\frac{1}{N})^{1/2}$ instead to get symmetry between the transform and its inverse. n_j represents photon counts with a Poisson distribution.

If using the central limit theorem, $[A_k]$ and $[B_k]$ have mean values of 0 and standard deviations $\sigma = (\frac{n}{2N})^{1/2}$ where $n = \sum \frac{n_j}{N}$. The amplitudes C_k can be calculated as in *equation 3.4*.

$$C_k = \sqrt{A_k^2 + B_k^2} \quad (3.4)$$

The mean value of $[C_k]$ is described by *equation 3.5*

$$\langle [C_k] \rangle = \sigma \sqrt{\left(\frac{\pi}{2}\right)} = \frac{1}{2} \sqrt{\left(\frac{\pi n}{N}\right)} \quad (3.5)$$

The power of each frequency can be calculated as the square of the amplitude and then plotted in a power spectrum, $[P_k] = [C_k^2]$. In a power spectrum, P_k is plotted against k (or $\nu_k = k/\tau N$, $k=2, \dots, N/2$) (Warner, 1988). The points after $N/2$ are a reflection of the $N/2$ first ones.

A more complex form to describe a light curve, e.g. a sum of many sine waves, gives harmonics of the fundamental frequency. The accuracy of the location of a peak is dependent of the length of the data train. A long pulse-train gives a greater accuracy and a narrower peak in the transform $\Delta f = \frac{1}{\Delta t}$ (Hellier, 2001). Another way is by using a larger telescope aperture. In the light curve, the detectability of the periodicity is dependent on the signal-to-noise ratio which is proportional to $n^{1/2}$. The discrete Fourier transform of the photon noise is a white spectrum which means that the amplitude is independent of frequency. The signal needs to have significantly higher amplitude than the highest noise peaks to be accepted as real. However, a low-amplitude periodicity seen in many data sets can still be of interest.

Correlation functions

A correlation function is produced when the intensity trace is shifted with a specific delay-time and multiplied by itself in an autocorrelation and with another function in cross correlation. The autocorrelation $Cr(\tau)$ can be described by *equation 3.6* where $I(t)$ is the intensity as a function of time and τ is the delay time.

$$Cr(\tau) = \int_{-\infty}^{\infty} I(t)I(t - \tau)dt \quad (3.6)$$

The crosscorrelation $CCr(\tau)$ between two functions g and h is described by *equation 3.7* (Bracewell, 1965). ($g \star h \neq h \star g$)

$$CCr(\tau) = g \star h = \int_{-\infty}^{\infty} h(t)g(t - \tau)dt \quad (3.7)$$

A more detailed description of the autocorrelation function of the weighted residuals $Cr(i)$ can be described as in *equation 3.8* (O'Conner et al., 1984).

$$Cr(j) = \frac{\frac{1}{m} \sum_i = n_1^{n_1+m-1} r(t_i)r(t_{i+j})}{\frac{1}{n_3} \sum_{i=n_1}^{n_2} [r(t_i)]^2} \quad (3.8)$$

where $n_3 = n_2 - n_1 + 1$. $Cr(j)$ is the correlation between the residual in channel i and the residual in channel $i+j$ summed over a selected number of i channels. j is set at $n_3/2$. m is equal to n_3-j and it varies for each sum. Each residual is perfectly correlated with itself giving $Cr(0)=1$. For an observed function $I_0(t_i)$ that has a calculated randomly scattered curve $Y(t_i)$, n tends to infinity and then $Cr(j)$ will go to zero ($j \neq 0$) (O’Conner et al., 1984).

3.3 Instrumentation

The correlation functions are proportional to the square of the intensity and this means that larger telescopes are much more sensitive to high-speed measurements than smaller ones. Large optical telescopes are needed to collect enough photons to detect fast variability in faint sources. Different photon-collecting instruments are on the market. CCDs dominate the optical region because of their high quantum efficiency but their quite long read out times make them difficult to use for measurements on very short time scales. Fast CCDs are under development but it seems that one must choose between speed and noise. Photocathode detectors (photomultipliers) can time individual photons with a high accuracy but they have a limit in quantum efficiency and in its extension towards infrared. An optimal photon-detector should have high quantum efficiency, an extension towards infrared and a time resolution of nanoseconds.

Silicon based avalanche photo-diodes (APDs) are the best candidates but they have some undesired effects such as that the electronic avalanche during the photon detection temporarily can cause light to be emitted from the detector surface. There is also a problem with their small sizes, e.g. in use at large telescopes. APD’s can be quenched which makes the dead-time shorter. Germanium APDs exist and they are more sensitive into the infrared (e.g. Duraffourg et al., 2001).

An APD can produce a huge amount of incoming data and there is a need for real-time data reduction. This can be done by a hardware correlator that calculates the correlation function. Such a correlator records the incoming photons and calculates the autocorrelation of the intensity in one channel coming from one light source or the cross correlation between different light sources in more than one channel. It is desirable to also have a history-recorder mode which counts the time differences between successive photons. Several correlators exist on the market and they are used in many different areas, e.g. medicine, biology and astronomy. Some are in forms of cards that can be inserted into the computer and some are external hardware units. It is desirable to have a portable correlator that is easy to integrate with rest of the equipment (the computers and photon-detectors). A portable external correlator that is connected to the USB port of a host computer has been used in this diploma work.

3.3.1 OPTIMA–Optical Pulsar TIMing Analyser

OPTIMA (Optical pulsar Timing Analyser) was designed and built by the Max-Planck Institute for Extraterrestrial Physics in 1996 for the purpose to study pulsars optically with high time-resolution and it was built to measure light curves from faint sources with $m = 25$. A secondary goal was to measure the light from compact binary systems with rapid brightness variations (Kanbach, et al., 2003). It was built to be portable and to serve as a guest instrument at different telescope (*Figure 3.1*) (Straubmeier et al., 2004).

OPTIMA measures the arrival times of every incoming photon with a time resolution of 4 microseconds. The absolute arrival time is needed to compare the measurements with that from other science group e.g. simultaneous X-ray measurements. The four main parts of the system are the APDs, the GPS receiver and the frequency time base, two personal computers (for data-acquisition and detector control), and a CCD camera for target acquisition. To optimize the

observations and maximize the signal-to-background ratio, a bundle of seven fibres is put in a hexagonal pattern in the focal plane of the telescope. A single fibre is placed one arc minute away from the bundle to measure the sky brightness. The fibres have different radii in both ends to make it easier to use at telescopes with different focal lengths. These tapered fibres have a diameter of 300 micrometers and are made of pure silica.

A 3-4 arcmin field on the sky is reflected by a slanted mirror into a focal reducer and then picked up by a CCD camera of type *SBIG ST-7* (*Santa Barbara Instrument Group*). The stars in the image are then identified and the main target can be found. The CCD camera can stand in as a guiding system at telescopes that don't have a guiding system for guest instruments. When the signal is pointed at the centre fibre, 98 % of the flux is detected in this channel. Each fibre is connected to an APD detector. The APDs have a quantum efficiency of 60 % in a wide wavelength range, 400-1050 nm. (*Figure 3.2*)

The APDs have to stay cool (-30°) and the bias voltage needs to be maintained at several hundred volts. The APDs operate in a quenched "Geiger counter mode" (a photon-initiated avalanche pulse is quenched by the instantaneous reduction of bias voltage). The APDs have a diameter of 0.2 mm and they can count at up to several 100 kHz. The APDs used are of type *SPCM AQR-15-FC* produced by *EG&G Laser Components* which has a dark count less than 50 Hz (Kanbach et al., 2003). The electronic signal from the APDs needs to be correlated with the timing from up to six different global GPS satellites at the same time. This is made on a hardware level by a GPS based high-frequency oscillator. Possibilities to store a large amount of data are necessary to enable observations with the OPTIMA detector system (Straubmeier et al., 2004). A rotating polarization filter of type *10K* from *Spindler & Hoyer* can be put above the fibre pick-up to measure polarized objects such as polars. A prism spectrograph with 4 output channels can also be used (Kanbach et al., 2003).

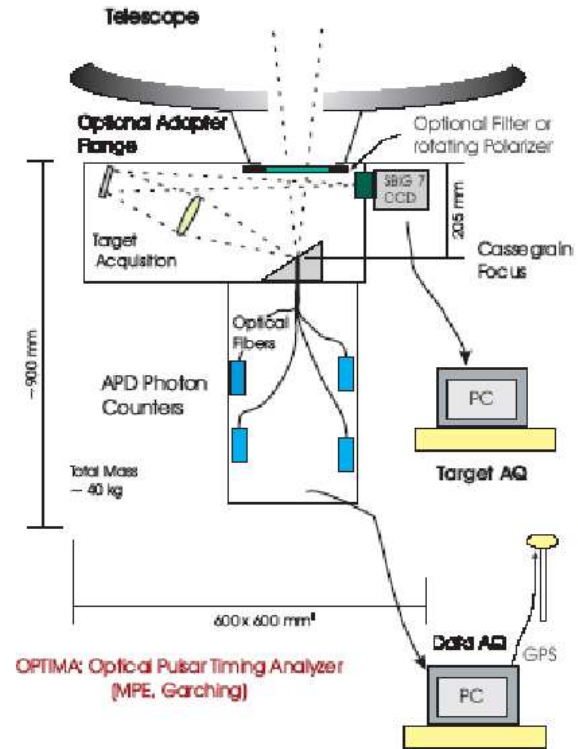


Figure 3.1: The OPTIMA system (Kanbach et al., 2003).

3.3.2 QVANTOS–Quantum Optical Spectrometer

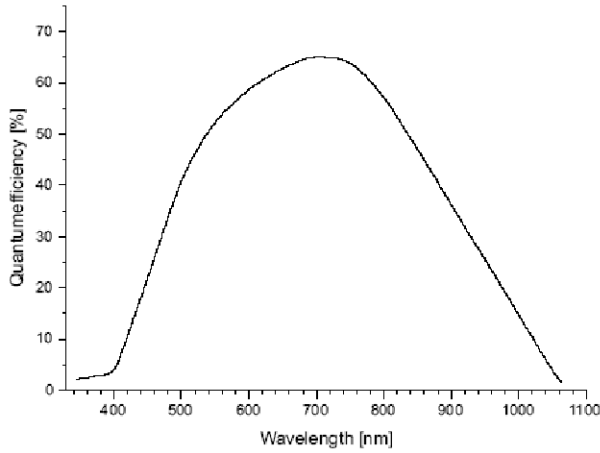


Figure 3.2: *Quantum efficiency for an APD of type SPCM AQR-15-FC produced by EG&G Laser Components (Straubmeier et al., 2004).*

Lund Observatory has designed an instrument to measure high-speed phenomena, *QVANTOS* (*Quantum Optical Spectrometer*). Its first version, *Mark I*, was used on La Palma (Dravins et al., 1997ab; 1998) to explore the atmospheric scintillations on short timescales. Before any accurate astrophysical measurements can be interpreted, it is necessary to understand what rapid variability can be induced by the terrestrial atmosphere. QVANTOS did measurements on La Palma at different times of the year, time of the night, different zenith distances and at different colours within the optical region. Data were recorded as correlation functions and then transferred into power spectra. The QVANTOS

system was designed for real-time computation of statistical functions of the photon arrival-times. An update of the QVANTOS system to a Mark II version included a purchase of a hardware correlator *Flex 01-05D* from the company *Correlator.com* in 2002.

3.3.3 Flex 01-05D and Development of the Software Program PhoCorr

The first part of this diploma work was to investigate how to use the correlator Flex 01-05D and to develop a control program, *PhoCorr*, for later use in observations of sources with fast variability. (Figure 3.3)

The correlator uses standard TTL-pulses to transfer data from the photon detectors. The so called "multiple-tau" method is used to calculate high-resolution correlation functions which means that the sample time and delay time are varied, in this case doubled, in consecutive channel segments. It uses so called "MT-64" (the first 64 channels are linear and then the sample time doubles every 32 data points), "MT-32" and "MT-16" schemes in the modes A, B and C where mode A is single correlation, mode B is quad correlation and mode C is dual correlation. The auto or cross correlation can be calculated in all modes with a minimum sample time of 5 ns. In all modes, the number of photon pulses within a certain time interval is registered and the intensity traces are then displayed in units of Hz as the number of photons divided by the time interval. The correlator can also be used in a *Photon History*



Figure 3.3: *The hardware correlator Flex 01-05D and the control program PhoCorr under development (Photo from the optics lab, Lund Observatory).*

Recorder mode and the time difference between successive photons is then recorded and transferred to the hard drive of the computer via USB. The system can be used up to count rates of many megahertz. (See *Appendix B* for more detailed hardware information)

Before any control program could be developed it was necessary to learn how the correlator operates. There was but little documentation and several tests were made in the process. One of the problems was the lack of information how the calculated correlation functions were normalized.

A couple of sample programs in VB (Visual Basic), C++ and LabVIEW were provided as an alternative to the existing software program for Flex 01-05D. The existing program *flex* was not adapted to astrophysical measurements and had some undesired functions such as tool-bars for use in medicine or biology-measurements. We used the LabVIEW sample-program *Flexx01* to build a control program for the correlator. LabVIEW is a graphical programming language that is produced by *National Instruments*. Two windows are used, the *front panel* that is the user interface and the *block diagram* where the functions can be linked together graphically with "wires". LabVIEW are mainly used for controlling external instruments. The control program *PhoCorr* was programmed to display the intensity traces and correlation functions in real time and to store the incoming data in a text file format, for further analysis.

The laboratory setup during the programming included APDs (from PerkinElmer). Thermoelectrically cooled APDs can detect photons in a wide wavelength range ($\sim 400\text{--}1060\text{ nm}$) and the quantum efficiency is approximately 70 % at 650 nm. An upper limit of the count rate is approximately 10 million detected photons per second and the dead time between the pulses is 50 ns. The APD voltage is required to be maintained at maximum +5 Volts¹.

Stray light from lamps in the room as well as light diodes were used as light sources. Tests were made by using a pulse generator that created pulses that were regulated in a chosen pattern by a word generator and then sent to the correlator. The word generator was in some cases connected to the light diode to simulate a variation that might be detected from astronomical sources.

Before any programming could be done it was necessary to learn how the LabVIEW programming language was constructed and the user manual was studied carefully before the sample program *Flexx01* could be understood. The sample program *Flexx01* was far from completed but the main functions as the *USB Initialize*, *Start*, *Update*, *Stop* and *Free*, existed and were put in a *Stacked Sequence Structure*.

PhoCorr was finished after approximately two months of testing and programming. Instead of one-user interface as in the program *flex*, four front-panels are used. The main front-panel creates one sub front-panel for each mode when specifying sample time, mode and cross or auto correlation. The intensity trace for channel A and B is displayed in all modes.

Data are saved in text files and the correlation functions consist of segments containing a certain number of channels depending on which mode was used. In single correlation, each segment consists of 1088 channels (608 and 288 channels in dual and quad mode). Maximum delay time, 183 min, is obtained in dual mode. The intensity traces is saved in all modes in addition to the correlation functions. Values are put in the first 24 channels depending on the value of the function *wait* in *PhoCorr*. The value was set to 1000 ms and this corresponds to the time in which the correlator gathers the intensity values for each segment. Data is collected in a channel during the time interval, 0.04194304 s ($\sim 50\text{ ms}$). A separate program *Photon* were used for the *Photon History Recorder mode* since no such function existed in the DLL-file for use when programming in LabVIEW.

A user manual was written, documenting the evaluation of the correlator and its control program *PhoCorr*. However, the manual is not comprehensive and there still are some unanswered

¹<http://www.perkinelmer.com>

questions concerning exactly how the correlation functions are normalized. (*See Appendix B for more detailed program information*)

Several experiments were performed during the process of understanding the basics of the correlator and to be able to make a useable control program. In some cases the instrumental setup included a word generator connected to a pulse generator and a light-emitting diode. APD detectors were then connected to the correlator. The word generator is using hexadecimals to create a word. Some examples of tests that were performed with the above mentioned instrumental setup can be studied in (*figure 3.4, 3.5 and B4*). *Figure 3.4 and 3.5* show double pulses from a light-emitting diode (LED) generated by a pulse generator. The pulse width can be seen at 55 ns. The distance between the pulses was chosen by a word-generator to be $1\ \mu\text{s}$ and the pulse-pair period is visible at $25\ \mu\text{s}$. Two components are seen in the peak at $25\ \mu\text{s}$ that are due to the period of the first-pulse pair and the first peak in the second pulse-pair and then the period of the first pulse-pair and the second peak in the second pulse-pair. The results of another test that was performed can be seen in *figure B4*. Stray light from the lamps in the room can be recognized in a correlation function as a 100 Hz oscillation at delay time $1 \cdot 10^{-2}$ s. The oscillation is due to the 50 Hz alternating current.

A more recent correlator model *Flex 03LQ-1* was obtained from the same company, Correlator.com in October 2004. It has a time resolution of ≈ 1.56 ns and intensity traces can be recorded with a minimum integration time of $0.1\ \mu\text{s}$. We have not yet been able to evaluate this correlator and unfortunately it could not be used in the observation campaign.

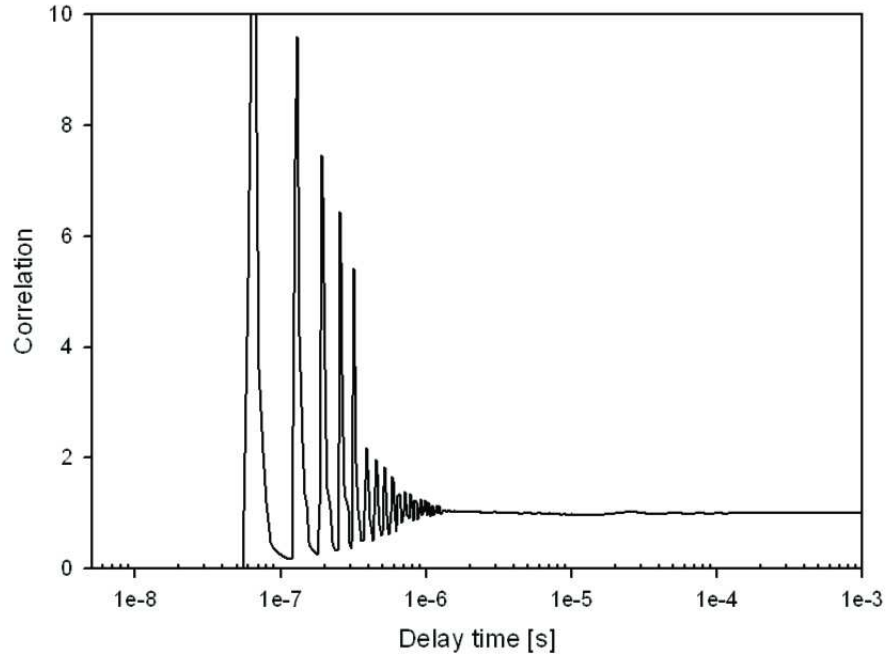


Figure 3.4: *Auto correlation of double pulses from a light-emitting diode. The pulse width can be seen at 55 ns. Optics lab, Lund Observatory, April 1, 2004.*

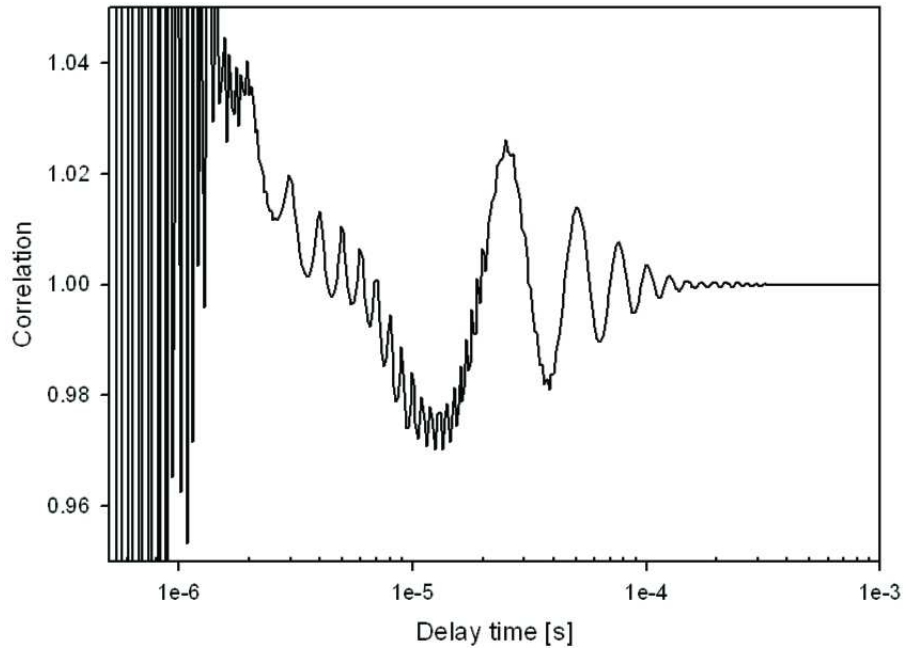


Figure 3.5: *The pulse-pair width can be seen at $1 \mu\text{s}$ and the pulse-pair period at $25 \mu\text{s}$. Optics lab, Lund Observatory, April 1, 2004.*

Chapter 4

Applications of High-Speed Astrophysics

4.1 Introduction

The second part of the diploma work was done in collaboration with the OPTIMA group. The correlator had been evaluated in the first part using the same type of avalanche photo-diodes from the company *PerkinElmer* as are used in the OPTIMA system. The compatibility of the OPTIMA system and the correlator Flex 01-05D was confirmed during three days of testing in Garching near Munich, June 2004 (*figure 4.1*) and a decision was made to join the OPTIMA group during an observation campaign at Skinakas Observatory on Crete/Greece in October 2004. Their main goal for the campaign was to test a new CCD camera and to prepare a forthcoming gamma-ray-burst campaign. Different compact objects as CVs, LMXBs, BHC-binaries and pulsars were also going to be observed, which agreed with our purpose of the campaign.



Figure 4.1: *Testing of the compatibility of the OPTIMA and Flex 01-05D systems in Garching.*

investigated.

The data were analyzed, especially for two objects, the cataclysmic variable SDSS J0155 and the black-hole binary Cygnus X-1. To confirm astrophysical origin of the variabilities, some

The preparations for the campaign started roughly one month before and suitable objects were selected. Simulations of the expected correlation functions were done for some objects using known light-curve data.

The campaign took place during October 10–25, 2004. Measurements of several compact objects were made and intensity traces and correlation functions were stored to be analyzed later. The main goal of this campaign was to test the correlator Flex 01–05D and its possibilities in observations of rapid variability in compact objects. Oscillations on different time scales were found during some measurements and their possible origins were later inves-

reference objects were investigated as well.

4.1.1 Skinakas Observatory

The main telescope at Skinakas Observatory was made by *DFM Engineering* and has an equatorial mounting. The size of the main and secondary mirror is 1.29 m and 0.45 m, respectively, and they are separated by a distance of ~ 2.4 m. To make the telescope stay on track, an auto-guider system uses an "off axis guiding" system made by *Baader Planetarium*. *Figure 4.2* shows OPTIMA mounted at the telescope.

The observatory is located in the central part of Crete, in the Ida mountains at an altitude of 1750 m (longitude $24^\circ 53' 57''$ East and latitude $35^\circ 12' 43''$ North).¹ *Figure 4.6* The seeing conditions of the site have been investigated by Boumis et al., 2001 using a two-aperture "Differential Image Motion Monitor" (DIMM). Their result showed that the seeing conditions do not usually change more than $0.3''$ during the night, and very good seeing conditions have been measured quite often ($0.4''$). The mean value is $\sim 0.6''$.

4.2 Preparations for the Observing Campaign



Figure 4.2: *Optima mounted on the 1.3 m telescope at Skinakas Observatory on Crete, Oct 23, 2004.*

The preparations started a month before the campaign and maps of the night sky from the observation site were obtained. The position of bright disturbing light sources as the city *Herakleon* and the bright moon had to be considered. Herakleon is situated in the north direction and its light could disturb observations in this region. The campaign would start at new moon. The moon would be visible low above the horizon in the second week and in the end of the second week it could disturb observations made in the southern part of the sky. The objects studied should not be fainter than $\sim 17^{th}$ magnitude to be possible to observe by the 1.3 m telescope.

Targets were selected and finding charts that covered an area of $10' \times 10'$ and $5' \times 5'$ were obtained². Among the chosen cataclysmic variables were some polars in which QPOs on the time scales of a few seconds had been found, e.g. EF Eri, VV Pup, AN Uma and HU Aqr. Some LMXBs and HMXBs were selected since they are well known to show millisecond phenomena. The millisecond Crab pulsar is one of few pulsars that is bright enough to be visible with a 1.3 m telescope and this was one of the targets as well. Another reason to observe the Crab pulsar is that it has been well studied and the results can

be compared with many other observations. The black-hole binary Cygnus X-1 is another bright and well studied source that was selected for the campaign. The selected objects are listed below in *figure 4.3* ("V" is the visual magnitude, "R.A." is in hours min s and "Dec." is in $^\circ ' ''$ and "Visible" denotes the local time of observability).

¹<http://www.skinakas.org.gr>

²Cadctfs Digitized Sky-Survey Interface, <http://www.dao.nrc.ca/cadbin/getdss>

Figure 4.3: *List of selected targets for the observation campaign.*

Target	R.A.	Dec.	V	Visible	Type
IW And	01 01 08.9	+43 23 25.7	≈ 11	20-05	Nova
V2275 Cyg	21 03 02.0	+48 34 52.9	≈ 10	00-05	Nova
HU Aqr	21 07 58.2	-05 17 39.0	15.3	20-00	AM Her
VV Pup	08 15 06.8	-19 03 18.0	14.5	03-05	AM Her
AN UMa	11 04 25.8	+45 03 14.0	14.5	03-05	AM Her
EF Eri	03 14 13.1	+22 35 42.0	13.7	00-05	AM Her
Crab Pulsar	05 34 31.9	+22 00 52.0	16.5	22-05	Pulsar
KV UMa	11 18 10.8	+48 02 11.2	≈ 14	03-05	BHC
Cyg X-1	19 58 21.7	+35 12 06.0	8.9	21-00	BHC
V404 Cyg	20 24 03.8	+33 52 04.0	12.8	21-00	LMXB
V406 Vul	18 58 41.5	+22 39 30.2	15.3	21-00	LMXB
X Per	03 55 23.1	+31 02 45.0	6.1	20-05	HMXB

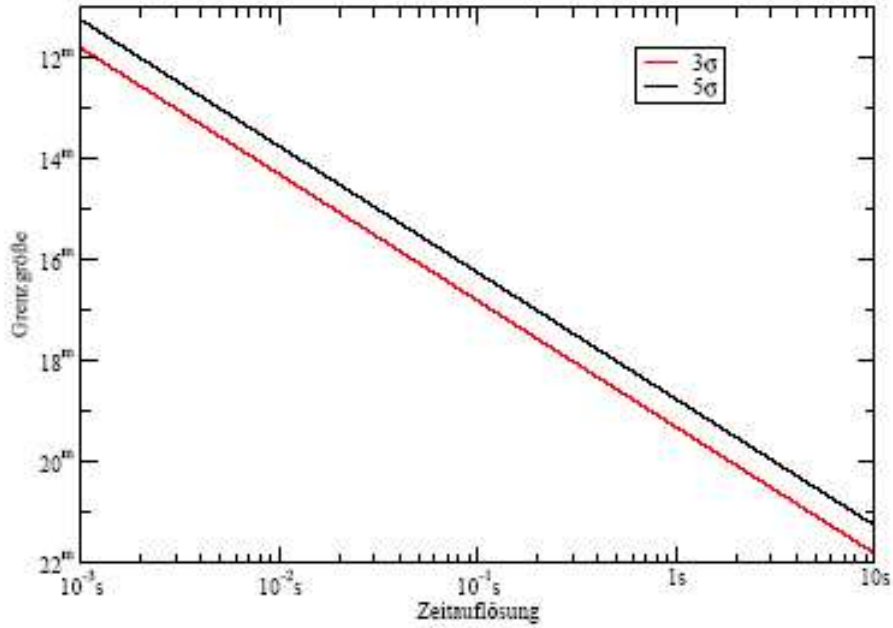


Figure 4.4: *Reachable magnitude limits at different time resolution with OPTIMA mounted at the 1.3 m telescope at Skinakas Observatory. (Stefanescu, 2003)*

The size of the photon-collecting area of the telescope is the greatest limitation of what can be detected. Reachable magnitude-limits using OPTIMA mounted at the 1.3 m telescope at Skinakas Observatory are plotted against time resolution in *figure 4.4* (Stefanescu, 2003). A time resolution higher than 1 s requires that the objects are brighter than the 17th magnitude. The QPOs found in some polars at a period of a few seconds must thus be at least of the $\approx 19^{\text{th}}$ magnitude or brighter to be detectable.

Simulations of the expected correlation functions using known light curves of some of the objects were done with the program *SimCalc* developed by Ricky Nilsson. (*Appendix A.2*) The

program displays the light curve, correlation function and power spectra. Known intensity data of the Crab pulsar was used to construct a light curve and its expected correlation functions and power spectra can be studied in (figure 4.5).

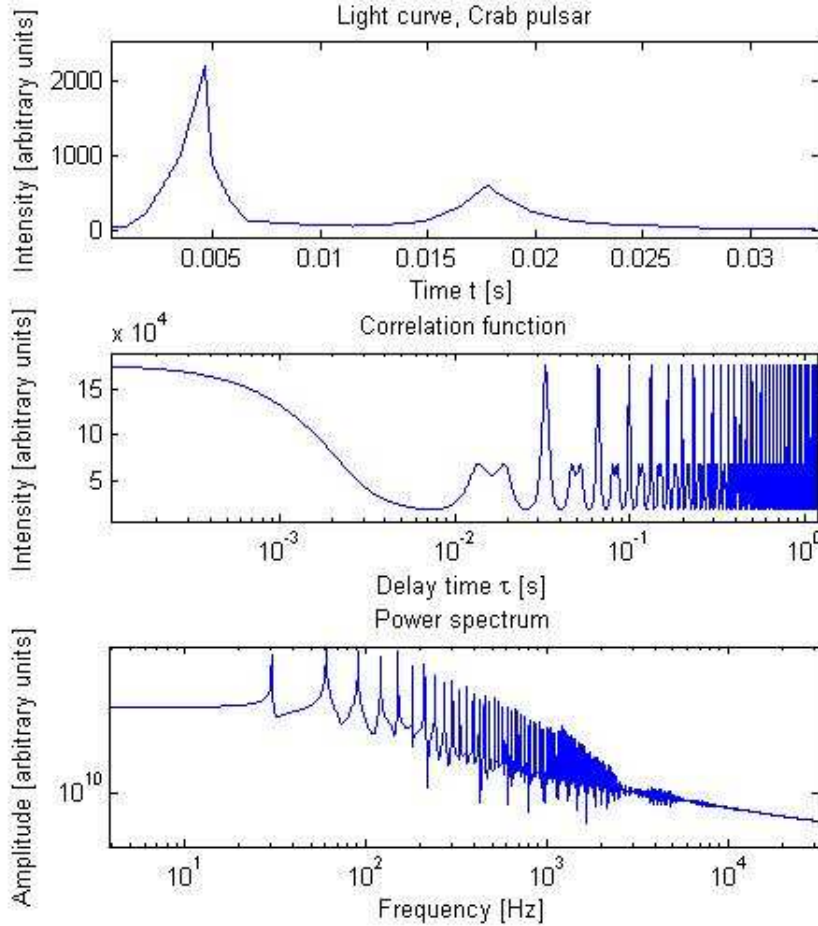


Figure 4.5: Simulations in the program *SimCalc* of the expected correlation functions and power spectra of the Crab pulsar using known light-curve data.

4.3 Observing Campaign at Skinakas Observatory

The campaign took place during 15 days in Oct 10–25, 2004 with eleven nights of observations. The first nights showed varying cloudiness, with most of the clouds below the observation site. During Oct 16–18 we experienced heavy wind that might have interfered with the observations and caused the telescope to vibrate. The following nights were clear with some thin, high clouds and the dome had to be shut down for some times due to humidity.

One of the eight fibres in the OPTIMA system was put at a distance of one arcmin from the bundle to measure the background sky level and two fibres were connected to the correlator, one displaying the source in correlator input channel A and one showing the background sky in channel B. The integration times of the measurements varied from 300–15000 s. Short integration times were used when searching for strong, fast variability in the correlation function. To



Figure 4.6: *The 1.3 m telescope dome at Skinakas Observatory on Oct 23, 2004.*

detect the variability on short time scales in e.g. the Crab pulsar, already a short integration time was sufficient. However, to get a signal with less noise a longer integration time was to be preferred. The highest resolution was obtained in single auto-correlation mode. Measurements of calibration stars were obtained for some of the objects.

4.3.1 Observed Sources

About a hundred measurements of about 25 objects were obtained during the campaign. The observed objects are listed in *figure 4.7* (No. is the number of integrations done. The sign, \star is put after information obtained from the *SIMBAD* data base, *Center for Backyard Astrophysics* or *CADC's Digitized Sky-Survey Interface* ³).

The observations started on Oct 13 and the first target to be observed was Cygnus X-1. The object was very bright (magnitude ≈ 10) and this measurement confirmed that the correlator did get a signal from at least one of the OPTIMA fibres. The Crab pulsar was the next object to be observed and the signal from different fibres were cross correlated to find out if there was any noticeable difference between them that could be detected in a correlation function. No obvious difference was found.

³<http://simbad.u-strasbg.fr/Simbad>, <http://cba.phys.columbia.edu/> or <http://cadwww.dao.nrc.ca/cadcbn/getdss>

The weather conditions changed on Oct 17 when we suddenly experienced heavy wind. Observations that evening showed the same kind of periodic oscillations at $\approx 5\text{--}50$ Hz in different sources such as V 404 Cygni and Cygnus X-1. The oscillations were clearly showing up in the auto correlation function when tapping on the OPTIMA box.

On Oct 18, a spectrograph was placed in the OPTIMA instrument box and the incoming light from the central fibre was spectrally dispersed through a prism into a four-fibre pickup, enabling broad-band colour measurements in red, yellow, green and blue. The different colours were cross correlated during measurements of the Crab pulsar. No significant differences could be detected in the correlation function when the fibres with different colours were correlated.

The oscillations that had been observed for some nights were found to be most prominent in zenith and much less pronounced when studying objects situated in other directions. The next evening, Oct 19, correlation functions of three field stars positioned at different angles from zenith were obtained in the search to find the rapid oscillations. The field stars studied are noted 2, 3 and 4 in *figure 4.7*. Oscillations at $\approx 20\text{--}50$ Hz could be detected in all measurements.

On Oct 21 a millisecond oscillation was found in some sources. A couple of tests were made to try to recreate the ≈ 2 kHz signal and flash lights were directed at the dome. The 100 Hz oscillation from the lamps was seen in some of the tests but none of the earlier observed oscillations could be found. Acoustic tests were also performed with a loudspeaker and a frequency generator at 2 kHz. The signal could then be detected in the correlation function.

No periodic variability could be observed in the measurement of any of the cataclysmic variables except for SDSS J0155. The seeing conditions were varying during the campaign and showed values as 2.1" in the beginning of the first week and 1.2" later in the second week.

4.3.2 Observations of SDSS J0155

The eclipsing polar SDSS J0155 was observed during three different integrations, the first in the late night of Oct 21 and the next two in the following evening. The integration time for the three measurements was as long as 10000 s and 15000 s. The reason for this was to be able to collect data for more than one period, polars have typical periods of ≈ 2 h. A ≈ 3 s oscillation was present at all measurements, and did not exist in the background noise or in the measurements of other sources obtained before and after SDSS J0155. The oscillation was strongest before and after the eclipse.

4.3.3 Observations of Cygnus X-1

Cygnus X-1 was observed and data were obtained during eleven occasions. The first two sets of data obtained in the early evening on Oct 13, were sampled during 300 s. Oscillations of ≈ 7 Hz and ≈ 48 Hz were found during the next measurement on the evening of Oct 18 but unfortunately these oscillations had been found in measurements of other objects earlier.

The next two sets of data, both of 600 s, were obtained in the late night of Oct 20. A distinct kHz oscillation was found at ≈ 1900 kHz (≈ 0.5 ms) in both sets of data but unfortunately, oscillations found in measurements of its calibration star could be identified as the same kind of variability. It was clear that Cygnus X-1 was not the origin of any of the variations found. Five sets of data were obtained in the auto-correlation mode the following evening, all with sample

times of 600 s. A kHz oscillation was present in Cygnus X-1 and its calibrations star again.

Figure 4.7: *List of observed objects during the campaign at Skinakas Observatory, Oct 2004.*

Target	R.A.	Dec.	V	No.	Type
Cyg X-1	19 58 21.7	+35 12 06	8.95 ★	11	BHC
V1674 Cyg	19 58 21.6	+35 13 00.7	9.62	3	Variable
Crab pulsar	05 34 44.51	+22 03 26.6	16.5 ★	20	Pulsar
Calibration, Crab Pulsar	05 34 01.1	+22 03 23.3	15.7	~ 5	Star
Calibration, Crab Pulsar	05 34 8.7	+21 59 33.3	-	-	Star
HU Aqr	21 07 58.3	-05 17 39.4	16.5	~ 25	CV
New CV in Pisces	00 25 11.2	+12 17 11.0	-	~ 10	CV
V404 Cyg	20 24 03.8	+33 52 03.2	11.5 ★	1	LMXB
Calibration, V 404 Cyg	20 24 01.3	+33 53 0.2	-	1	Star
X Per	03 55 23.1	+31 02 45.0	6.1 ★	2	HMXB
Field star 1	00 11 27.7	+29 36 07.9	-	1	Star
Field star 2	00 00 32.2	+17 05 32.8	10.1	~ 5	Star
Field star 3	21 57 56.3	+29 11 40.6	10.26	2	Star
Field star 4	21 08 05.9	-05 17 04.4	10.73	2	Star
4 U0115+63, Field star 5	01 18 32.0	+63 44 24.0	-	2	Star
BL Lac	22 02 43.3	+42 16 39.9	14.5	1	Quasar
Calibration star, Cyg X-1	22 52 05.24	+16 32 24.8	9.26	2	Star
V2275 Cyg	21 03 02.0	+48 45 52.9	~ 18	1	Nova
SDSS J0155	00 55 43.38	+00 28 06.7	14.7 -17.6 <i>star</i>	3	AM Her
V1974 Cyg	20 31 31.7	+52 37 50.8	4.5 ★	1	Nova
LW Cam	07 04 09.95	+ 62 03 27	~ 19 ★	1	AM Her

4.4 Data Analysis

The stored data from the campaign were in the form of intensity traces and correlation functions saved in text files by the program PhoCorr. (*See Chapter 3.3.3 for more information*) The data displaying programs SigmaPlot and MATLAB (MATrix LABoratory) were used for the data analysis.

Light curves were constructed from the stored intensity traces. The intensity file consisted of segments containing a number of channels depending on which mode was used. For each segment, values were put in the 24 first channels and the remaining channels were filled with zeros. The channels with values had to be selected and transformed in SigmaPlot and/or procedures in MATLAB were constructed to extract the data and to get a file consisting of one data string of intensity values. Data are collected in each channel during the time interval 0.04194304 s and the channel numbers were incremented with this value to get a sample-time x-axis. In the cases for data sets obtained in the single-correlation mode, the fibre containing the source signal was connected to the correlator input-channel A, and the signal from the background was put in channel B. The intensity of the background sky could then later be subtracted from the intensity of the source. The MATLAB smoothing procedure *'rloess'* (*Robust Local Regression Smoothing Procedure*), which uses a second degree polynomial at a specified number of data points, in this case 10 data points, were used to smooth the intensity data. A light curve could now be plotted with the smoothed intensity versus sample time. (*Appendix A.1*)

The intensity data were in some cases used to calculate correlation functions and power spectra. This was done in SigmaPlot and/or MATLAB. The standard procedure in both programs is to choose the number of data point to 2^N where N is an integer. An *fft* function then calculates the Fourier function of the data string and the power is calculated as the square of the Fourier function, $(\text{abs}(\text{fft}(\text{data})))^2$. SigmaPlot uses the transform *POWSPEC.XFM* to calculate the power spectral density. A frequency scale is generated by using a sampling frequency set to 24. The length of each data point is $1/24$ s and thus 24 channels have a total time-duration of 1 s. Each point of the light curve has a sample time of ≈ 50 ms which means that variability shorter than this can not be detected in the intensity data. The MATLAB program SimCalc was in some cases used during the data analysis. (*Appendix A.2*)

The correlation functions obtained by the correlator have a minimum sample time of 5 ns which gives a much higher temporal resolution than if using the intensity data to calculate the correlation functions. The correlation functions were saved in a text file containing one segment for each stored second of observation. Depending on which mode was used, the segments consist of a different number of channels. This gives the possibility to choose and plot the correlation function that has been built up after an exact time with an accuracy of one second. Data after a given segment were then extracted and plotted against delay time. The y-axis represents the correlation ($\approx \text{Intensity}^2$) and the x-axis show the delay time measured in seconds. *Figure 4.8* shows auto-correlation functions of the Crab pulsar and its calibration star measured on Oct 19, 2004. *Figure 4.8* can be compared with the simulated correlation function in *figure 4.5*. A structure at shorter time-scales in the correlation function obtained with the correlator can be seen below the millisecond scale. If this is actual periodicities in the Crab pulsar or if this is the "after pulsing" from the APD detector is not possible to find out in an auto correlation function. A cross correlation between several detectors could possibly reveal periodicities in the Crab pulsar at timescales less than milliseconds.

The correlation functions were plotted after desired delay times and then smoothed in SigmaPlot using a "running average" over 5 data points. (*See Appendix B for further information about PhoCorr and the correlator*)

4.4.1 SDSS J0155, Analysis of Observations

The eclipsing polar SDSS J0155 was found to be fainter than the 16^{th} (maybe 18^{th}) magnitude, indicating that the system was in a low state during the observations. The period and eclipse length of the system was measured directly in the light curve from Oct 22 to be 5176 ± 120 s ($\sim 86.3 \pm 2$ min). This can be compared with the period 87.13 min measured by Szkody et al. (2002). A mean value of the eclipse width was measured to be 304 ± 6 s. The mass of the secondary star can be estimated by the equation $M_2 \approx 0.065 P^{5/4} M_{\odot}$ (the period should be expressed in hours: Hellier, 2001). If using this approximation the secondary mass is $\approx 0.1 M_{\odot}$. Wiehahn et al. (2004) presents a mass of the secondary of $(0.07 \pm 0.03) M_{\odot}$ and Dubkova et al. (2003) approximated the secondary mass to be $0.17 M_{\odot}$. Several system parameters can be approximated by using the mass of the primary and secondary star. A primary white dwarf in a polar is assumed to have a mass in the range of $0.3 M_{\odot}$ - $1.4 M_{\odot}$ (Dubkova et al., 2003). Wiehahn et al. (2004) assume a mass of the primary star to be $0.66 M_{\odot}$ - $0.94 M_{\odot}$. If using a mass of $0.8 M_{\odot}$ and a q value of 0.09 (the mass ratio between the binaries) the separation between the stars can be calculated as in *equation 2.5* giving a value of a of approximately $4 \cdot 10^8$ m.

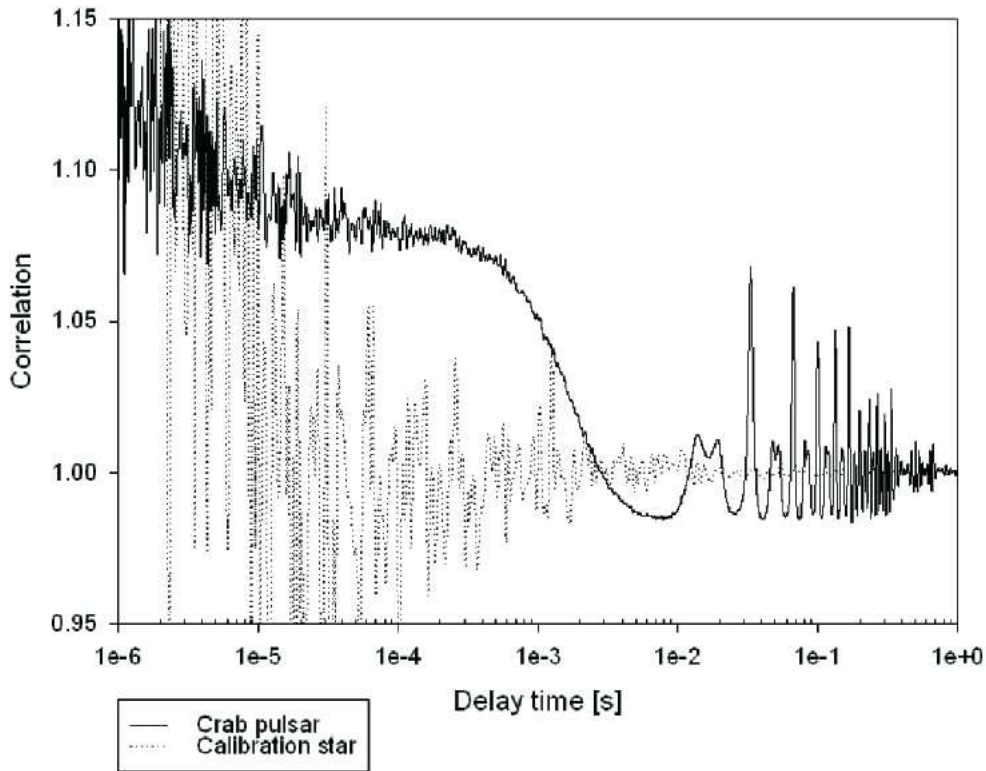


Figure 4.8: *Auto-correlation function of the Crab pulsar and its calibration star obtained on Oct 19, 2004.*

Intensity Measurements

Three sets of data were obtained with the program PhoCorr and the intensity traces were extracted in MATLAB, corrected for the background and smoothed with the function 'rloess'. Intensity versus time and phase was plotted. One eclipse is seen in the light curve obtained on Oct 22 (*figure 4.9*). Another light curve from the next evening includes three eclipses before dawn (*figure 4.10*). Wiehahn et al. (2004) have calculated the inclination of the system to be $85^\circ < i < 90^\circ$. This means that most of the light from the white dwarf and parts of the accretion stream is eclipsed by the red dwarf. Notice the rise in intensity around the eclipses that indicates that the accretion region is visible just before and after the eclipse. For half of the orbit the column is hidden behind the limb of the white dwarf and a decrease in intensity can be seen between the eclipses. This feature is characteristic for a polar with one leading accretion pole. A shallow dip can be seen in phase 0.92-0.95 just before the eclipses. (*Figure 4.11*) This feature was also observed by Dubkova et al. (2003) and Schmidt et al. (2004) during low state. An assumption by Schmidt et al. (2004) was that this could be due to absorption by the accretion stream.

Schmidt et al. (2004) have constructed a picture of the geometry in the area of the eclipse (between phase, 0.88–1.09) for the system. Earth lies in the plane of the paper with the observer orbiting the binary in a clockwise direction. A white dwarf of mass $0.6 M_\odot$ and a main sequence secondary of mass $0.11 M_\odot$ that fills its Roche lobe are assumed. The funnel starts its self-eclipse ingress at phase 0.88. The dip due to absorption by the accretion stream can be seen at phase 0.94 and at phase 0.97 is the primary eclipse egress. The white dwarf is fully eclipsed at phase

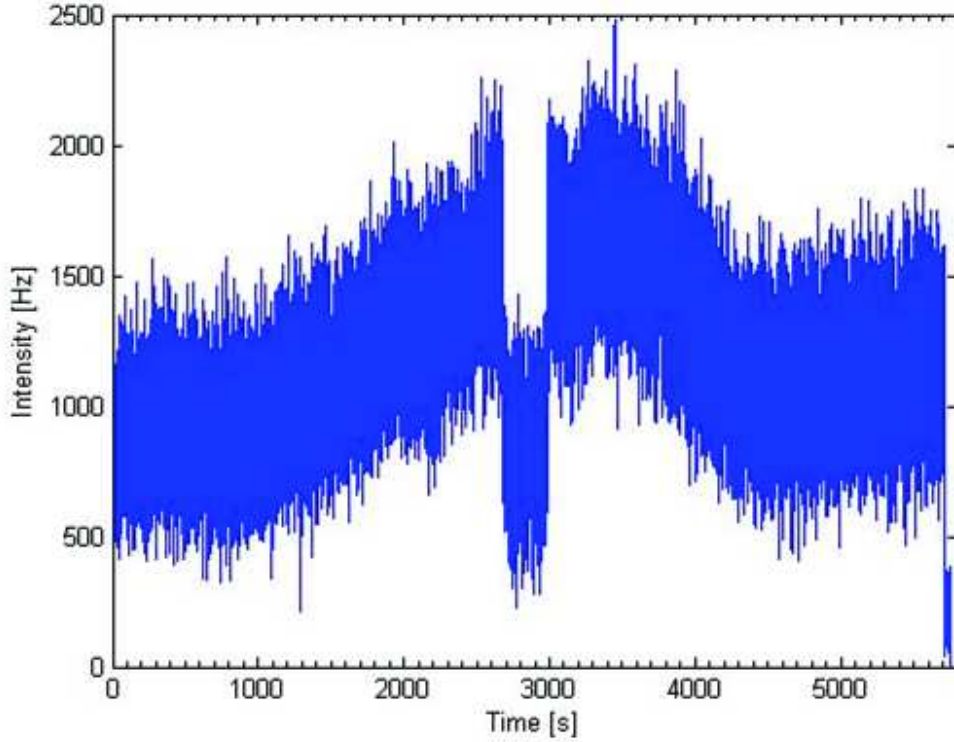


Figure 4.9: *Light curve of SDSS J0155 obtained on Oct 22, 2004.*

1.0. At phase 1.03 occurs the primary eclipse egress and the funnel is full exposed at phase 1.09. The figure by Schmidt et al. 2004 is put together with a plot of the central part of the light curve measured on 22 Oct, 2004. *Figure 4.11*

Search for a Quasi-Periodic Oscillation

A weak QPO with a period of ≈ 3 s was detected in the correlation function in all data sets obtained for SDSS J0155. The signal was not found in any other sources and could not be detected in the background signal. The QPO amplitude varied with the orbital phase and was strongest just before and after the eclipse but much less prominent between the eclipses.

Auto-correlation functions obtained by PhoCorr at different phases were plotted and a very weak but persistent signal could be detected at ≈ 2.6 – 2.7 s. The correlation functions obtained after a certain integration time correspond to a certain phase in the period of SDSS J0155. Correlation functions were obtained from before, between and after the eclipses. *Figure 4.12* show the smoothed auto-correlation functions as a black line and the non-smoothed auto-correlation functions as a grey line. At the top left is a peak visible as obtained on Oct 22. The background auto-correlation function acquired simultaneously can be studied at top right and as expected, no peak is visible. The next six correlation functions were obtained the following evening. The peak is visible at the same delay time during the period. The "overtones" of the oscillation are visible after the peak.

To rule out the possibility that the ≈ 3 s oscillation was present in any of the other sources, correlation functions of the objects obtained before and after the measurements of SDSS J0155, V2275 Cyg, the Crab pulsar, V1974 Cyg and LW Cam were investigated. No such oscillation

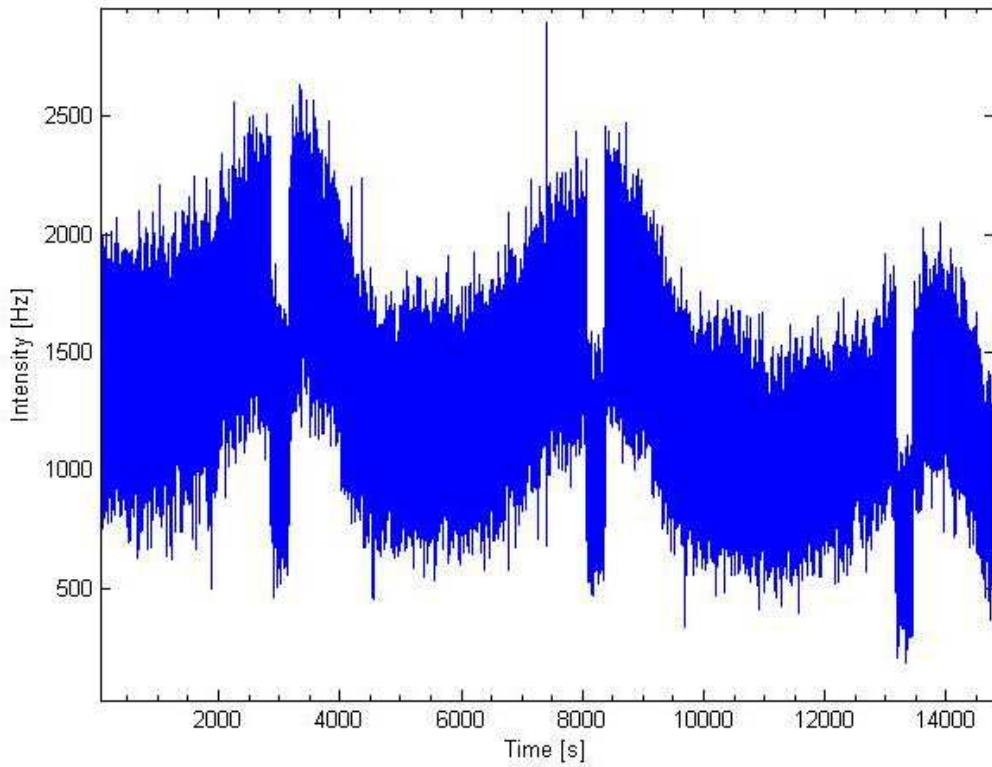


Figure 4.10: *Light curve of SDSS J0155 obtained the evening after the light curve shown in figure 4.9.*

was found in any of those objects as can be seen in *figure 4.13*.

The search for the ≈ 3 s oscillation continued and power spectra were obtained from the light-curve data. The data were divided into different segments and then the procedure followed as described earlier. Power spectra were obtained for segments of usually 600 s from before, and after the eclipse, during the eclipse and in between the eclipses. A peak at ≈ 0.35 – 0.38 Hz can possibly be distinguished in most data sets from just before and after the eclipse. In some, but few cases a peak is visible during the eclipse. A low peak can in some cases possibly be observed between the eclipses when the accretion column is supposed to be behind the white dwarf. Another peak is visible at ~ 0.1 Hz but this feature disappears during the eclipse and becomes less prominent after the eclipse. This feature was not further investigated. *Figure 4.14–4.23*

Further analyses were performed and light-curve segments of 600 s, displaced for every 300 s were extracted from the intensity data. The program SimCalc calculated the correlation functions and power spectra of each segment. The weak oscillation was difficult to find in most of the correlation functions and power spectra calculated by SimCalc but a bump at ≈ 2.6 s can be seen in a segment obtained just before the eclipse (*figure 4.24*).

The ≈ 3 s oscillation is very weak but persistent and it is detected at the same delay time in all correlation functions. QPOs of a few seconds have been observed from polars (e.g. VV Pup and EF Eri) and are thought to originate from oscillating blobs in the accretion column. The accretion column of SDSS J0155 is self eclipsed for part of the orbit but a weak QPO is detected even between the eclipses when the column is supposed to be behind the white dwarf.

As mentioned in *chapter 2.2.5*, Wiehahn et al. (2004) found in their polarimetric observations of SDSS J0155 that the circular polarization plot (*figure 2.6*) shows both negative and positive polarization. They discussed whether this should be interpreted as a two pole accreting system or if it could be that the shock column is tall enough to be partly observed even when it is behind the limb of the primary. A change in sign of the circular polarization could happen if the magnetic field lines are facing away from the observer which would be the case if the column could be seen from behind the limb. (Wiehahn et al., 2004) This could explain why the QPOs are present for more than half of the period. The QPO could possibly also be observed in the power spectra during the eclipse. It is possible that some parts of the accretion region still can be visible during the eclipse. The possibility that the QPOs have another origin than the star itself cannot completely be ruled out. However, the ≈ 3 s oscillation was not detected in any other object and it is on a slightly different time scale than the other observed oscillations. Further analysis must be performed to confirm the origin of the 3 s oscillation in SDSS J0155.

4.4.2 Cygnus X-1 and Telescope Vibrations

The intensity traces from eleven measurements of Cygnus X-1 were extracted and plotted in MATLAB and the data were smoothed with the function 'rloess'. All measurements except for one were made in single auto-correlation mode and thus there were no background intensity-data that could be subtracted from the intensity traces. Cygnus X-1 is much brighter than the sky background and therefore a subtraction would not change the light curve significantly. Light-curve data from all measurements of Cygnus X-1 were extracted and plotted. (*Figure 4.25*) The correlation functions obtained by PhoCorr were extracted and plotted in SigmaPlot. Two peaks at ~ 0.02 s and ~ 0.14 s (~ 48 Hz and ~ 7 Hz) can clearly be detected in the correlation function of CygnusX-1 from Oct. 18. (*Figure 4.26*) The 7 Hz signal had been detected since Oct. 17 and the oscillations in the correlation function of Cygnus X-1 were compared with auto-correlation functions of V 404 Cygni and its calibration star (*figure 4.27 and 4.28*). The 7 Hz-variation and oscillations on similar time scales are visible in the correlation functions of Cygnus X-1, V 404 Cygni and its companion star.

There had been some reasons to believe that the oscillations could depend on telescope angle and it had been noticed during some measurements that the oscillations increased at some specific telescope angles. The result of the field-star test described in *chapter 4.3.1* showed oscillations of about tens of Hz in all stars, shifting in amplitude. However, there was no connection found between telescope angle and oscillation frequency. Two measurements were made of field star 2 showing that the oscillations were changing in frequency from time to time, independent of position (*figure 4.29, 4.30, 4.31 and 4.32*).

Correlation functions from Oct 21 show another periodic variation as mentioned in *chapter 4.3.3*. This kilohertz oscillation can be studied in *figure 4.33 and figure 4.34*.

Figure 4.33 shows the attempt of finding the origin of the oscillations using lamps. The 100 Hz variation from the lamps can clearly be detected.

Millisecond QPOs have been observed since a couple of decades in Cygnus X-1 (*figure 2.12*) and it can be a major confusion if something else can cause oscillations on the same time scale besides the source itself. Oscillations were found at different time scales from ≈ 5 –50 Hz to ≈ 2

kHz. In the search to find some further explanations tests including e.g. lights were performed. The dome lights did not seem to interfere with the measurement and the only oscillation seen was the expected 100 Hz oscillation from the lamps. Lamps from Herakleon city that could clearly be seen in the northern part of the sky could not possibly cause any of the variations detected. No 100 Hz oscillation was seen in any observations and there were no obvious difference in the observed oscillations when the telescope was in the south or north direction. The field-star tests showed that the telescope might cause oscillations on time scales of $\sim 5\text{--}50$ Hz. It is known that larger telescopes vibrate at typical frequencies between $\sim 10\text{--}50$ Hz ⁴ and therefore telescope vibrations is a plausible explanation of these oscillations. We experienced heavy wind during some of the nights and there is a possibility that this can have affected the telescope in some way.

Kristian J et al., 1989, found an extremely rapid periodic oscillation from the supernova 1987 A. The signal suggested that the pulsar rotated about 1970 times per second and this was the fastest rotating pulsar ever seen. However, a year later it was confirmed that the rapid oscillation that had been detected actually came from a television camera, situated inside the telescope to transmit an image of the sky. This confirms the importance to understand what is causing variability on the short time-scales that can interfere with the observations. It is important to study sources of error that can conflict with the measurements before any significant astronomical conclusions can be drawn.

⁴<http://www.mailbag.com/users/ragreiner/vibrations.html>

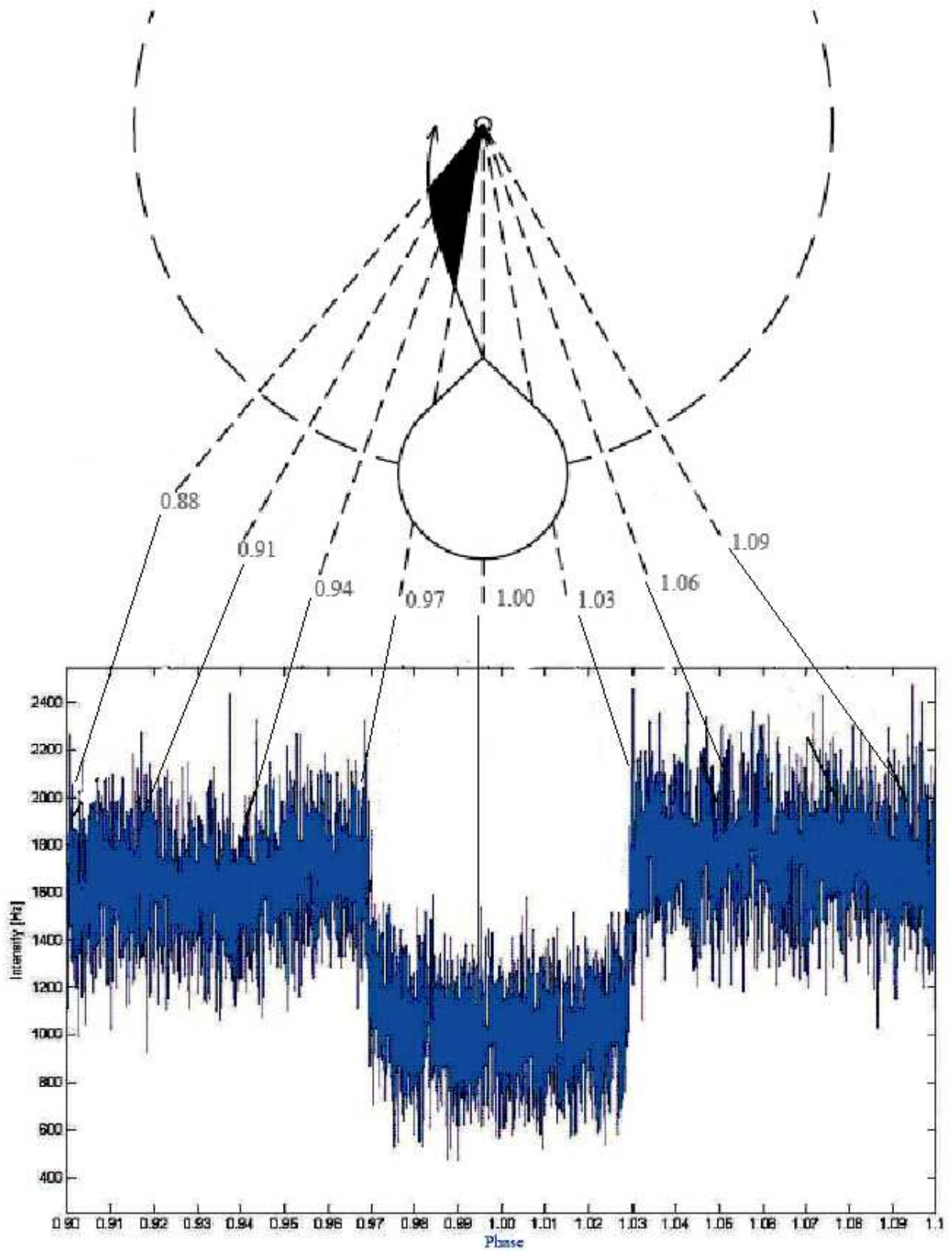


Figure 4.11: The light curve surrounding the eclipse of SDSS J0155 obtained on Oct 22, 2004, is shown together with a figure by Schmidt et al. (2004), showing the geometry of the system near the eclipse.

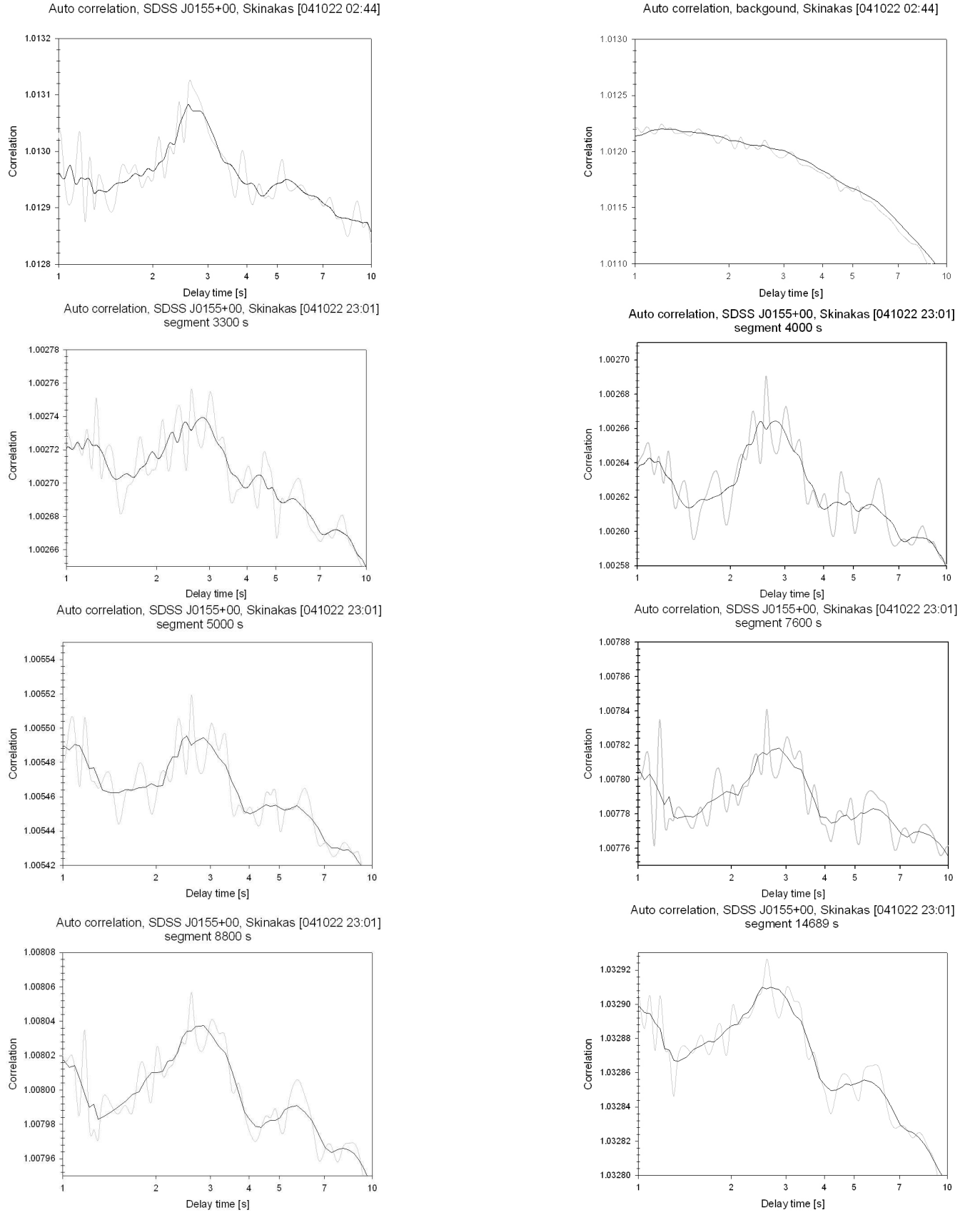


Figure 4.12: Auto-correlation functions of SDSS J0155. Notice the bump at $\approx 2.6\text{--}2.7$ s.

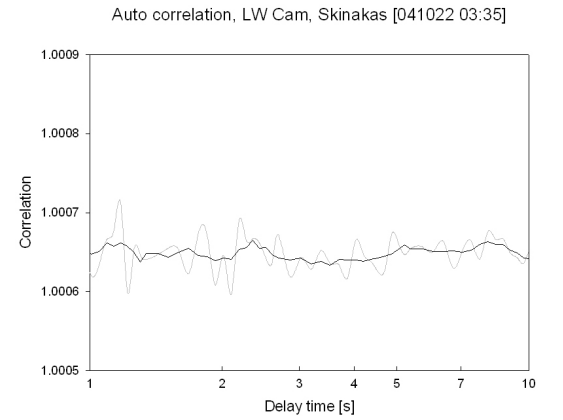
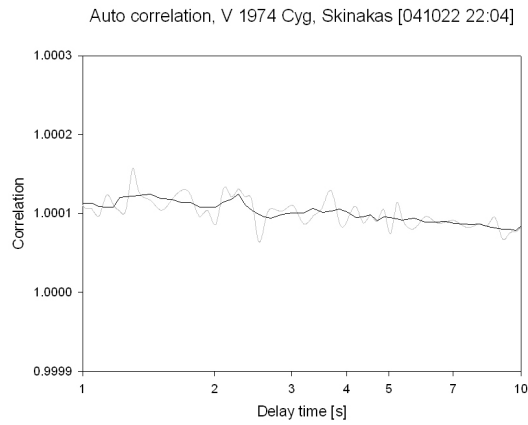
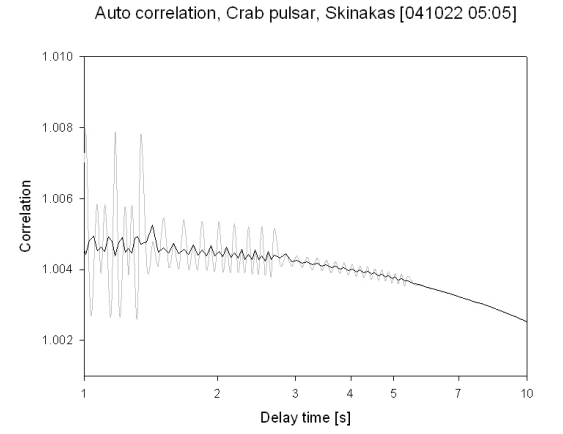
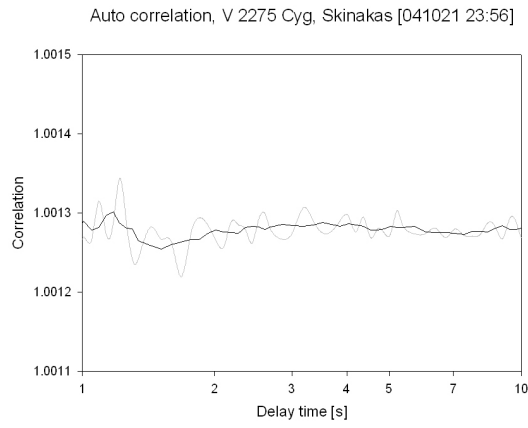


Figure 4.13: *Auto-correlation functions of some objects obtained before and after the measurements of SDSS J0155 in the search for the origin of the ≈ 3 s oscillations.*

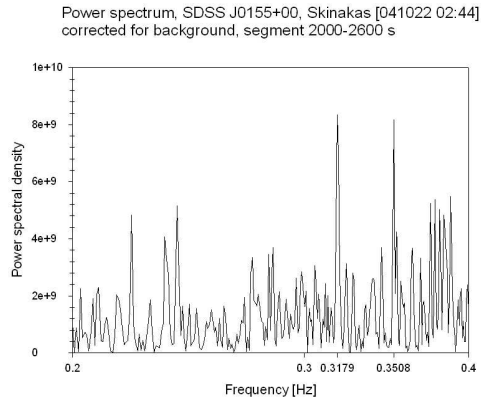


Figure 4.14: *Between eclipses.*
No prominent peak is seen.

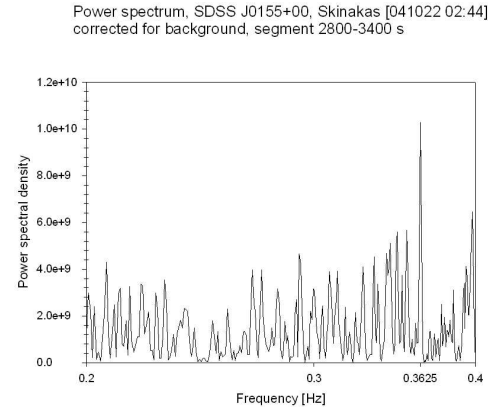


Figure 4.15: *Before the eclipse.*
A peak is seen at 0.36 Hz.

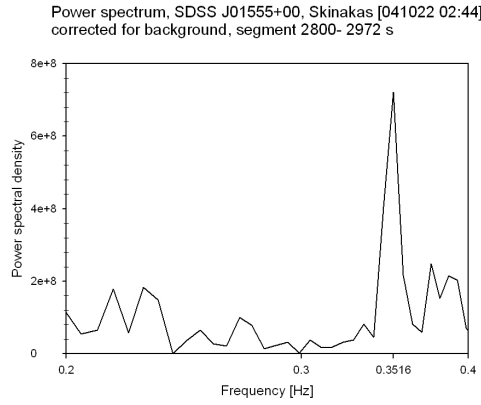


Figure 4.16: *During the eclipse.*
A peak is seen at 0.35 Hz.

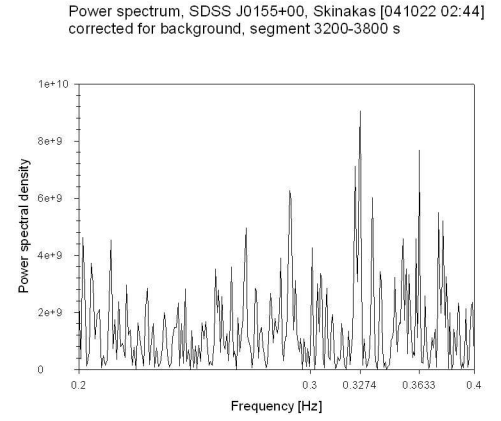


Figure 4.17: *After the eclipse.*
A peak is seen at 0.36 Hz.

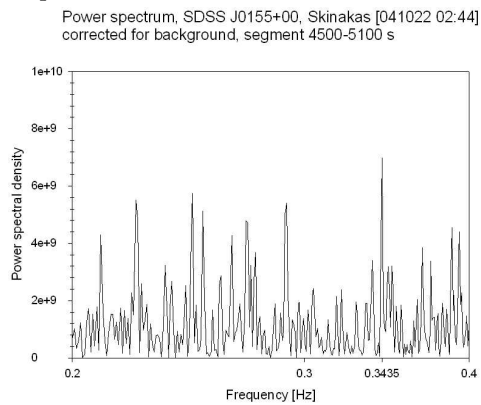


Figure 4.18: *Between eclipses.*
Low peaks are seen at ≈ 0.37 – 0.38 Hz.

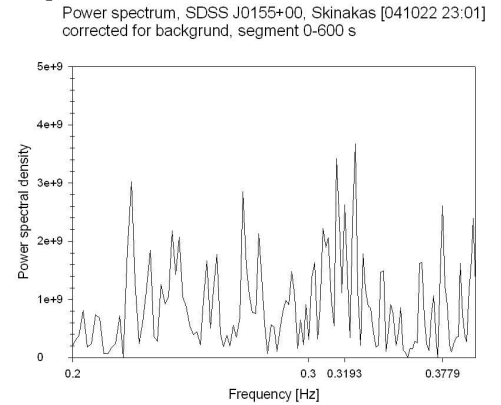


Figure 4.19: *Between eclipses.*
A low peak is seen at 0.38 Hz.

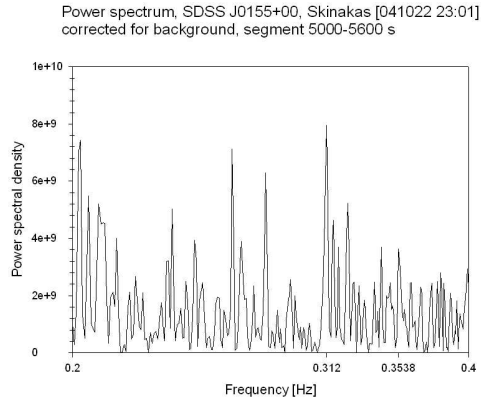


Figure 4.20: *Between eclipses. No peak is seen.*

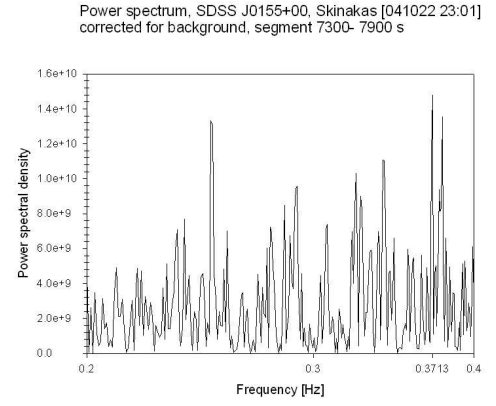


Figure 4.21: *Before the eclipse. A peak is seen at 0.37 Hz.*

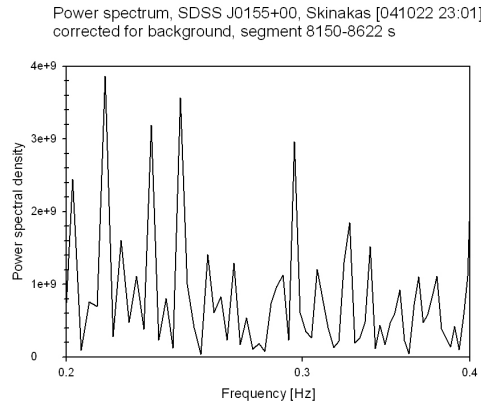


Figure 4.22: *During the eclipse. No peak is seen.*

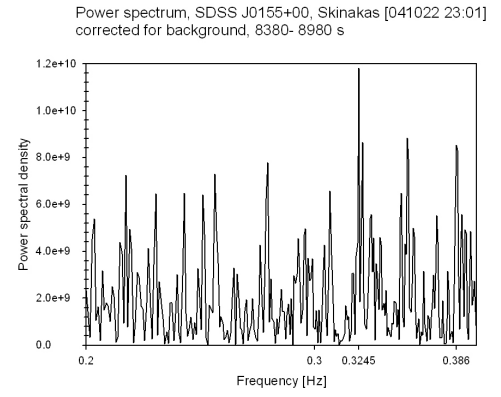


Figure 4.23: *After the eclipse. Peaks are seen at ≈ 0.32 Hz and 0.38 Hz.*

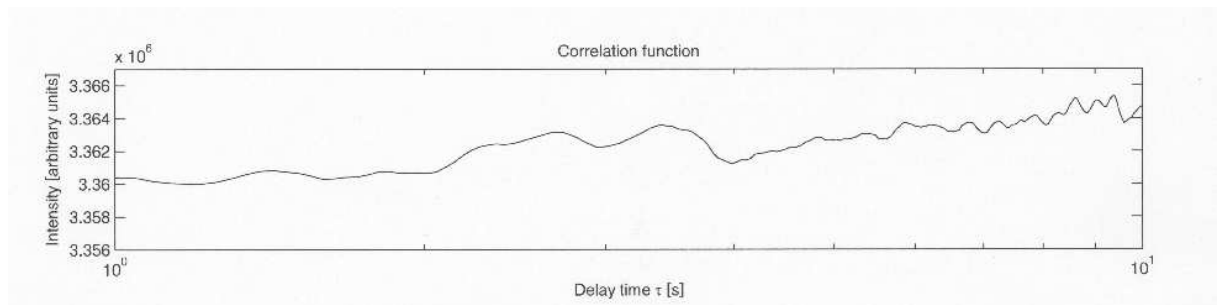


Figure 4.24: *A bump at ≈ 2.6 s seen in the correlation function of SDSS J0155 calculated by the program SimCalc.*

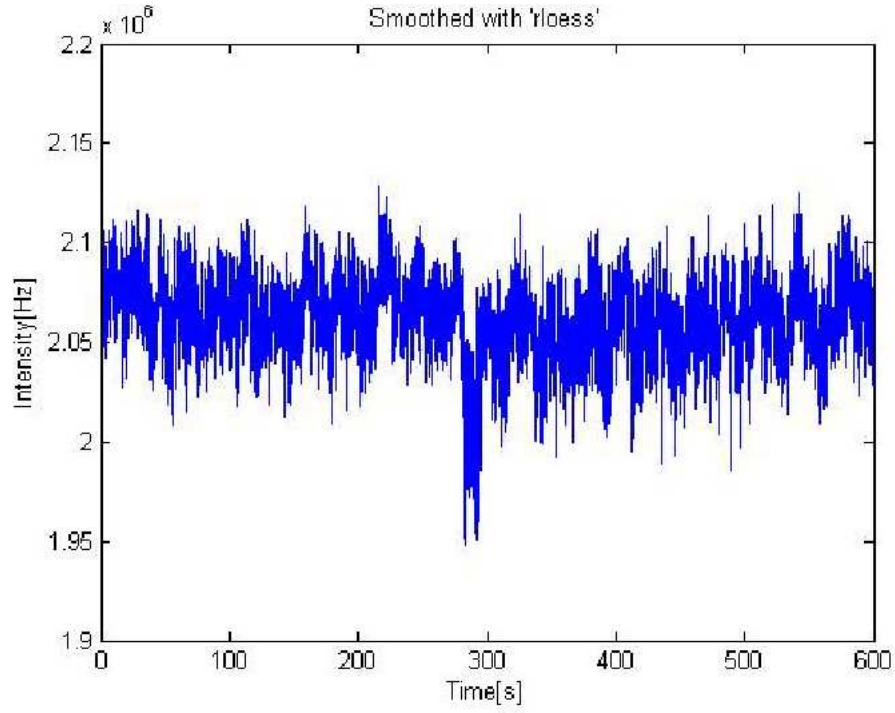


Figure 4.25: *Light curve of Cygnus X-1. The decrease in intensity is due to a small cloud in the line of sight at ≈ 300 s, Oct 21, 2004.*

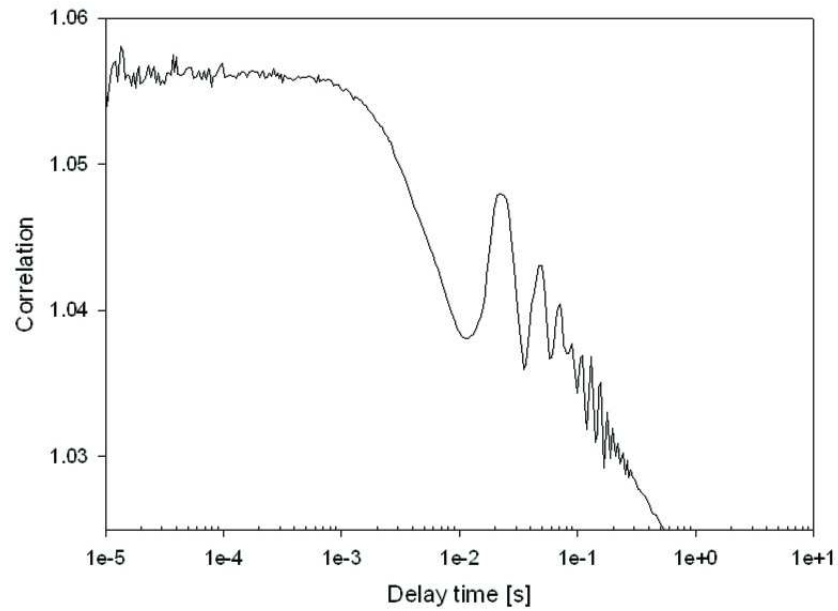


Figure 4.26: *Correlation function of Cygnus X-1. Two peaks at ≈ 40 Hz and ≈ 7 Hz are present, Oct 18, 2004.*

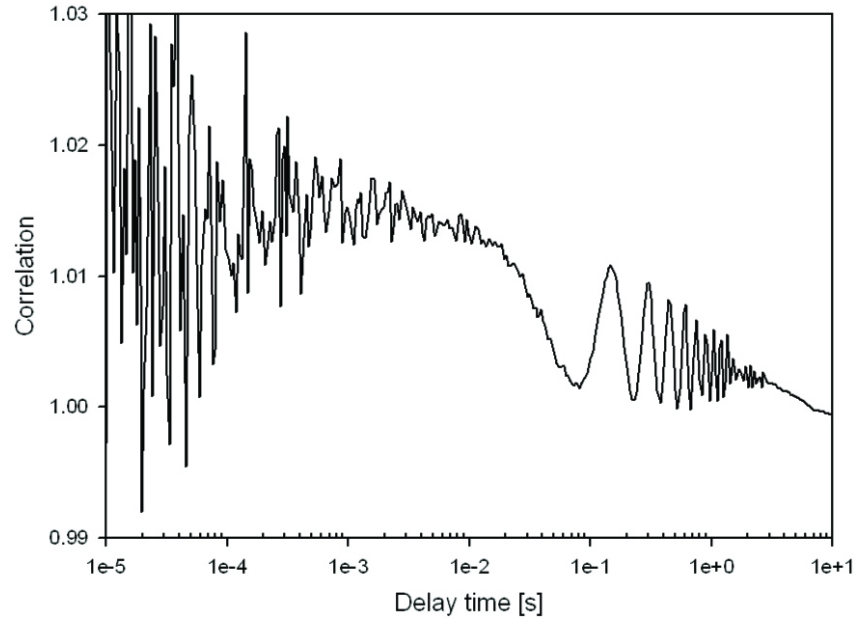


Figure 4.27: *Auto-correlation function of V 404 Cygni. Two peaks at ≈ 7 Hz and ≈ 1 Hz are present, Oct 17, 2004.*

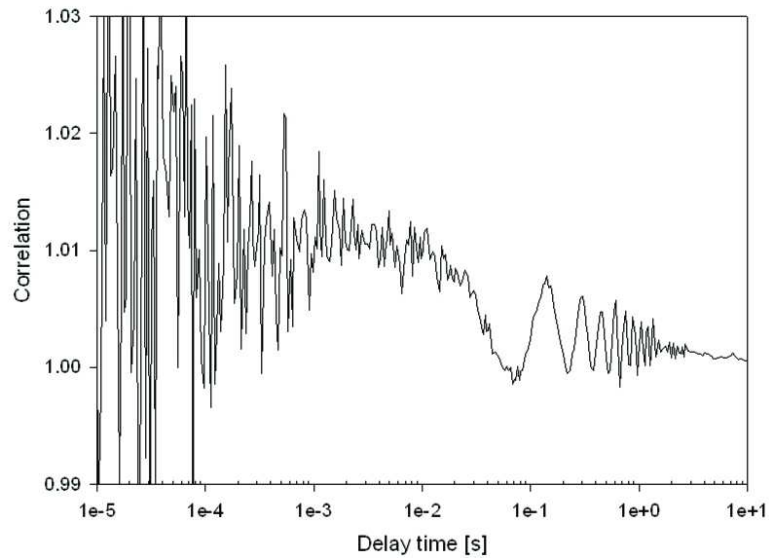


Figure 4.28: *Auto-correlation function of a calibration star to V 404 Cygni. Two peaks at ≈ 7 Hz and ≈ 1 Hz are present, Oct 17, 2004.*

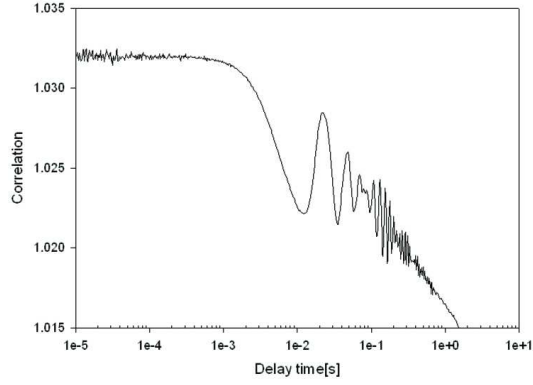


Figure 4.29: *Auto-correlation function of field star 2. Peaks are seen at ≈ 45 Hz and ≈ 5 Hz, Oct 19, 2004.*

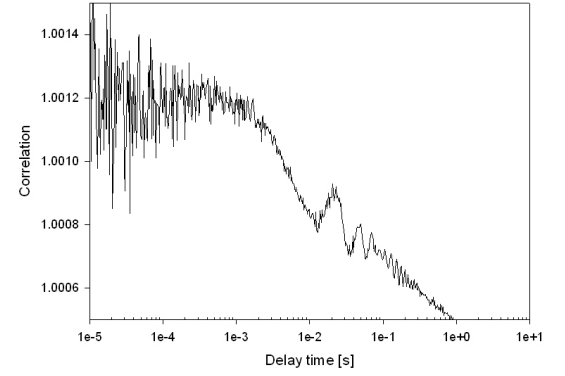


Figure 4.30: *Auto-correlation function of field star 3. Peaks are seen at ≈ 45 Hz and ≈ 7 Hz, Oct 19, 2004.*

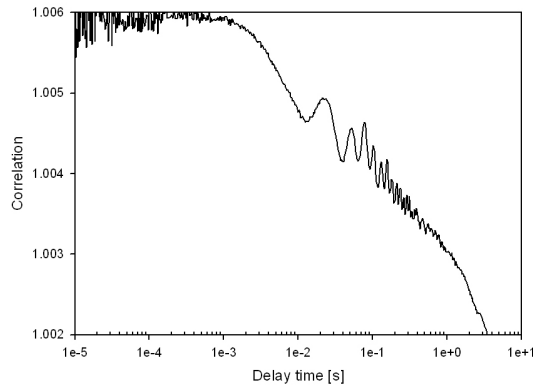


Figure 4.31: *Auto-correlation function of field star 2. Peaks are seen at ≈ 48 Hz and ≈ 14 Hz, Oct 19, 2004.*

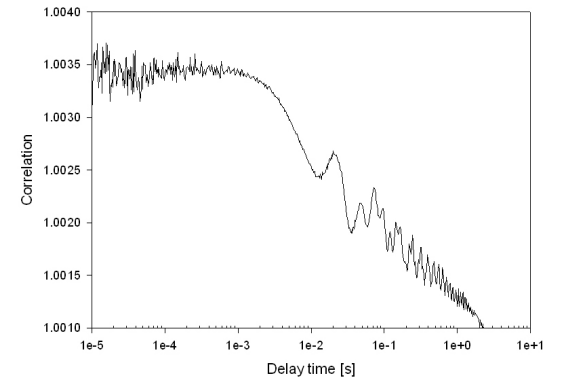


Figure 4.32: *Auto-correlation function of field star 4. Peaks are seen at ≈ 48 Hz and ≈ 14 Hz, Oct 19, 2004.*

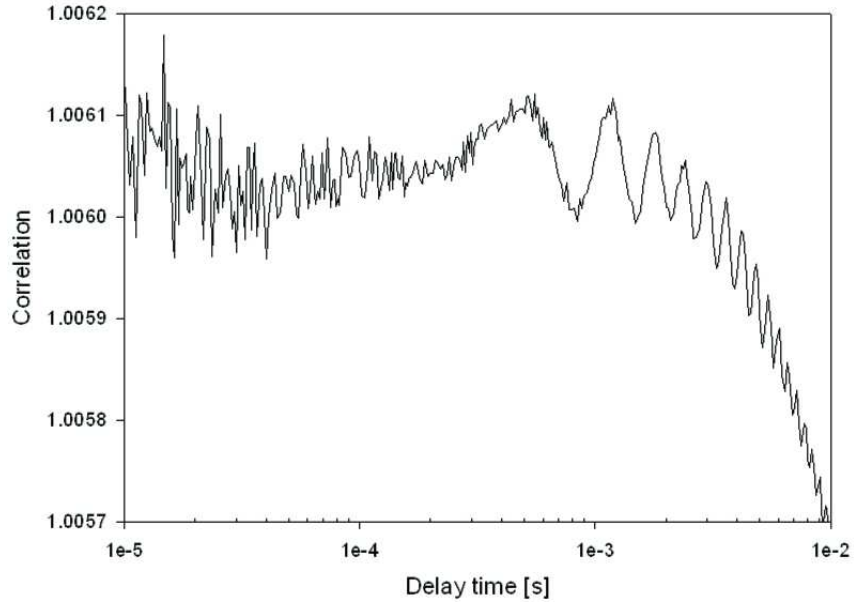


Figure 4.33: *Auto-correlation function of Cygnus X-1. A millisecond oscillation can be seen at 1.876 kHz, Oct 21, 2004.*

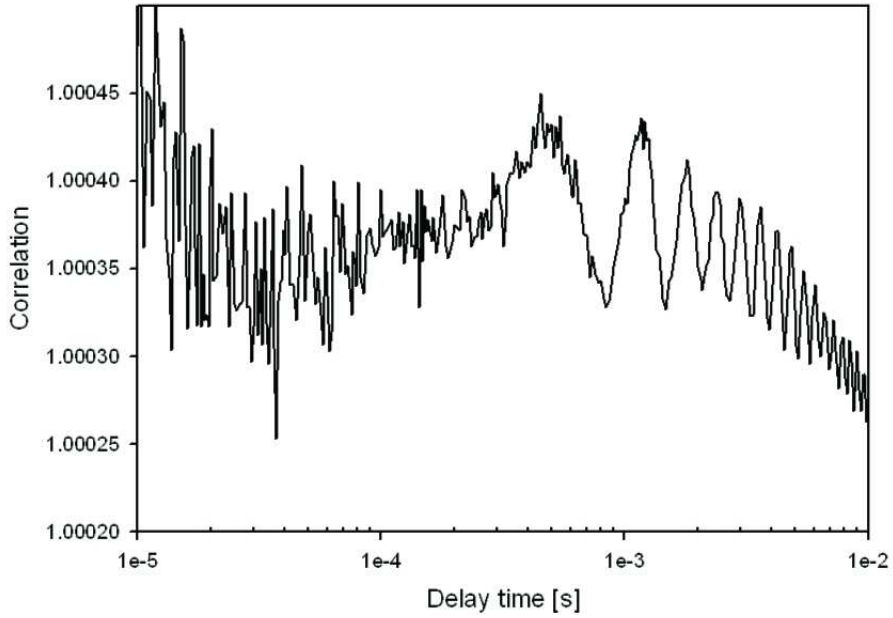


Figure 4.34: *Auto-correlation function of a calibration star to Cygnus X-1. The millisecond oscillation is present, Oct 21, 2004.*

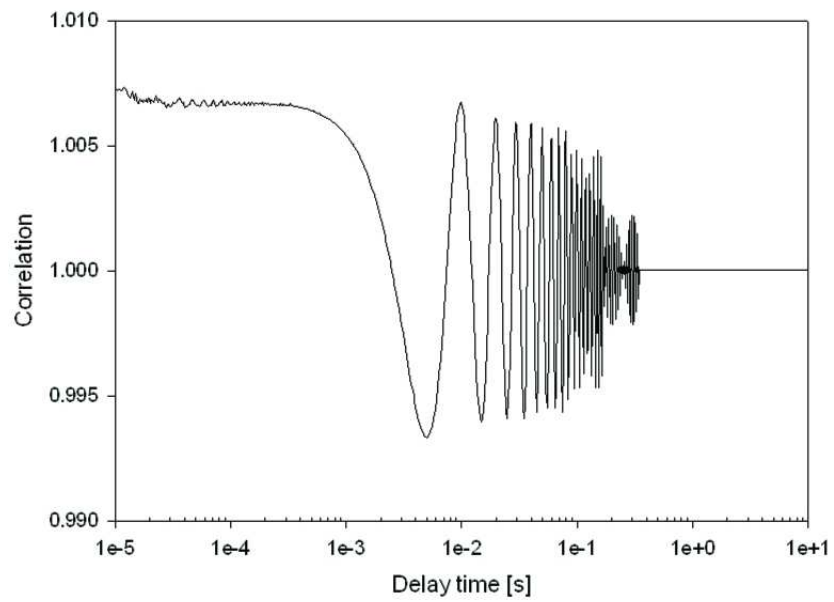


Figure 4.35: *Auto-correlation function showing a 100 Hz oscillation from the dome lights, Oct 21, 2004.*

Chapter 5

Summary and Possible Future Projects in High-Speed Astrophysics

5.1 Summary

The main goal of this diploma work was to explore and develop optimal methods for observing rapid variability in compact objects. A major part of the work involved developing a control program for the correlator Flex 01-05D and testing its possibilities in actual astronomical observations of such sources.

Phenomena on short time-scales detected as quasi-periodic oscillations (QPOs), are observed in compact binaries. The oscillations are thought to originate from the inner parts of the accretion region. If an accretion disc is present as in the case of low-mass X-ray binaries and black-hole candidate binaries, the oscillations might originate near the innermost stable orbit. Within this radius the material is accreting onto the primary compact object. In magnetic cataclysmic variables the strong magnetic field of the primary is preventing the formation of an accretion disc. The accretion stream from the secondary star must follow the field lines and will hit the primary star in the magnetic poles where oscillations are created near the impact region.

A system for high-speed measurements, QVANTOS, has been developed at Lund Observatory and an update of the system included a purchase of a hardware correlator, Flex 01-05D, from the company Correlator.com. The first and major part of the diploma work was to develop a control program for the correlator Flex 01-05D. Its basic control program flex, was not adapted to astrophysical measurements and it was desirable to create a program that could be used for our observations. This was done by enhancing a sample program developed for use in the LABVIEW programming environment. Before any programming could be performed, the correlator was evaluated and several tests were made to understand how it operated. It was also necessary to learn the LABVIEW programming language to be able to construct a useable control program. The system setup included instrumentation such as avalanche photo-diodes (APDs), a pulse generator and a word generator. Light sources as stray light from the lamps in the room as well as photo diodes was used. The correlator calculates the single or cross correlation of the photon stream in some of the chosen modes; single, dual or quad. Tests were performed by using a pulse generator which creates pulses that were modified in a particular pattern by a word generator and then sent to the correlator. The control program PhoCorr was developed to display and store the incoming data more easily. A user manual was written, documenting the evaluation of the correlator and its control program PhoCorr (*Appendix B*). However, the manual is not comprehensive and there still are some unanswered questions concerning how the correlation functions are normalized.

In the second part of the diploma work the correlator and the control program were used and its possibilities were tested in actual astronomical observations. Collaboration with the OPTIMA group at MPE, the Max-Planck Institute for Extraterrestrial Physics in Garching, gave an opportunity to perform astronomical observations of compact objects. The compatibility of the correlator with their APD-detector system, OPTIMA was tested and the two systems were found to be fully compatible. An agreement was made to join the group at an observation campaign at Skinakas Observatory on Crete in October 2004. Observations were made at the 1.3 m telescope and measurements of several compact objects were obtained. Correlation functions and power spectra were calculated and analyzed for several objects, in particular for the cataclysmic variable SDSS J0155 and the black-hole candidate Cygnus X-1.

The eclipsing polar SDSS J0155 was observed on three different nights, and a ≈ 3 s QPO was found during all measurements. Although the signal had very low amplitude and could barely be distinguished from the noise level, it was persistent in all measurements. The QPO could be detected for most of the period but was varying in amplitude. No similar oscillation was detected in any other object or in the background measurement. QPOs of a few seconds have been observed in polars such as VV Pup and EF Eri and are assumed to be created e.g. when illuminated blobs of matter are oscillating up and down in the accretion column. In SDSS J0155 the accretion column is self eclipsed and hidden behind the white dwarf for half of the orbit but the QPOs could be detected even when the accretion column is supposed to be behind the limb of the primary. Wiehahn et al. (2004) found both negative and positive circular polarization from SDSS J0155. This may occur if a tall shock column could be seen even from behind the limb of the white dwarf. If this is the case, then it is possible that the QPOs could be present even when the column is self eclipsed by the primary. The decrease in amplitude of the QPOs between the eclipses could then be explained by the fact that only parts of the column can be observed. Further analysis must be performed to determine the origin of the ≈ 3 s QPO, and an instrumental origin of these oscillations can still not be ruled out. Oscillations of a few seconds can not be referred to as "high-speed astrophysics" but it demonstrates the ability of the system to easily detect periodic oscillations in real time.

Apparent QPOs in the frequency range of ~ 5 –50 Hz and a ≈ 2 kHz oscillation were found in the correlation functions obtained of Cygnus X-1. However, oscillations in the same frequency range could also be detected in some of the other sources and it was soon clear that the rapid variations couldn't possibly originate from Cygnus X-1 itself. To determine the origin of these oscillations observations of field stars situated at different angles from zenith were made. Oscillations were found in the same frequency range as before (~ 5 –50 Hz) indicating that the telescope might have something to do with the oscillations found in this frequency range. It is known that larger telescopes vibrate and show periodic oscillations in the frequency range of Hz and tens of Hz. We experienced heavy wind during some of the nights that might have interfered with our measurements. It is important to investigate all sources of error that might inflict with the observations before any significant conclusions of astronomical interest can be drawn.

5.2 Future Projects

Analysis of some of the measurements shows that it is indeed possible to perform high-speed observations on a rather small telescope and still get valuable information. The low-amplitude oscillation found in SDSS J0155 could barely be detected and to be sure of its existence and its origin further analyses of the measurements and maybe more observations have to be performed. If using a larger optical telescope, it could be possible to detect phenomena on even shorter time scales. When reaching a time resolution of nanoseconds, correlation between individual

photons can be measured to get quantum mechanical statistics of the photons. This could lead to a greater understanding of the properties of light. The number of photons collected rises quickly with the size of the photon collecting area. The correlation is proportional to the square of the intensity and with a very large photon collecting area it is understandable that higher time resolution can be reached. Advantages of larger telescopes (operating with adaptive optics) also include a higher spatial resolution and some compact binary systems might be resolved. Lund Observatory in collaboration with the OPTIMA group has suggested performing the same kind of observations that have been done at Skinakas Observatory on the 11 m telescope SALT (Southern African Large Telescope) in the nearer future. The ongoing project of ESO, (European Southern Observatory), OWL (Overwhelmingly Large Telescope) involves the planning of a 100 m telescope. Measurements of high time resolution on such a large telescope would more than favor the study of quantum optics and high-speed astrophysics such as the search for **rapid events in compact binaries**.

Acknowledgements

I would like to thank Dr. Gottfried Kanbach and the rest of the OPTIMA group at MPE (Max-Planck Institute for Extraterrestrial Physics in Garching) for their hospitality during our visit in Garching and for the great opportunity to join them on the observing campaign on Crete. Special thanks to Fritz Schrey whose fantastic 6 o'clock dinners made us stay alive upon the barren mountain for weeks and thanks to Alexander Stefanescu who inspired us all during the nights to perform exciting observations. It was very valuable to be able to test the correlator in actual astronomical observations and this has enabled further work.

I would also like to thank my traveling partners, Ricky Nilsson and our supervisor Prof. Dainis Dravins for great company and nice conversations during the long nights at Skinakas Observatory over many cups of tea. This adventure would not have been possible without a creative supervisor who did not only give us the experience of performing observations but also gave us an insight in the great culture of Crete and in that of Germany during visits to a number of 'Biergarten" in Garching and Munich.

Very special thanks to my roommate Ricky who has an enormous patience and always have time to answer my questions.

At Lund Observatory, research engineer Bo Nilsson is thanked for advice and help with electronics in the optics laboratory.

Finally I want to thank my boyfriend Edward Birch-Iensen for his fantastic support during this diploma work.

Bibliography

- Abramowicz M.A., Wlodzimierz and Kluzniak, 2003, astro-ph/0312396
- Boumis P., Steiakaka A., Mavromatakis F. et al., 2001, astro-ph/0111022
- Bracewell R., 1965, *The Fourier Transform and its Applications*, Mc Graw-Hill
- Bursa M., Abramowicz M.A., Karas V. et al., 2004, *Astrophys. J.*, Vol. **617**, p. 45
- Caput C., Bloom E., Cominsky L. et al., 2000 *Astrophys. J.*, Vol. **541**, p. 1026
- Dolan J.F., 2001, *Publ. Astron. Soc. Pacific*, Vol. **113**, p. 974
- Dravins D., 1994, *ESO Messenger* No. **78**, p. 9
- Dravins D., Lindegren L., Mezey, E. et al., 1997a, *Publ. Astron. Soc. Pacific*, Vol. **109**, p. 173
- Dravins D., Lindegren L., Mezey E. et al., 1997b, *Publ. Astron. Soc. Pacific*, Vol. **109**, p. 725
- Dravins D., Lindegren L., Mezey E. et al., 1998, *Publ. Astron. Soc. Pacific*, Vol. **110**, p. 610
- Dubkova D.N., Kudryavtseva N.A. and Hirv A., 2003, *Inf. Bull. Var. Stars*, No. **5389**
- Duraffourg L., M  rolla J.M., Goedgebuer J.P. et al., 2001, *IEEE J. Quant. Electronics*, Vol. **37**, p. 75
- Giannios D. and Spruit H.C., 2004, *Astron. Astrophys.*, Vol. **427**, p. 251
- Gierlinski M. and Zdziarski A.Z., 2003, *Mon. Not. R. Astron. Soc.*, Vol. **343** p. 84
- Hellier C. 2001, *Cataclysmic Variable Stars, How and Why they Vary*, MPG Books Ltd, Bodmin
- Jaschel C. and Jaschel M., 1995, *The Behaviour of Chemical Elements in Stars*. Cambridge University Press
- Karas V., 1999, *Publ. Astron. Soc. Japan*, Vol. **51**, p. 317
- Kanbach G., Kellner S., Schrey F. et al., 2003, *SPIE*, Vol. **4841**, p. 82
- Kristian J., et al, 1989, *Nature*, Vol. **338**, p. 234
- Kundt W., 1999, *Mem. A.A.It.*, Vol. **70**, p. 1105
- Larsson S., 1995, Buckely & Warner, eds. *ASP Conf.* Vol. **85**, p. 311
- Mauche C.W., 2002, *Astrophys. J.*, Vol. **580**, p. 423
- Miller M.C., 2003, *Astro-ph*/0312449
- O'Conner D.V. and Phillips D., 1984, *Time Correlated Single Photon Counting*, Academic Press
- Rezzolla L., Yoshida S., Maccarone T.J. et al., 2003, *Mon. Not. R. Astron. Soc.* Vol. **344**, L37
- Sazonov S.Y. and Sunyaev R.A., 2001, *Astron. Astrophys.* Vol. **373**, p. 241
- Schmidt G.D., Szkody P., Homer L. et al., 2004, astro-ph/0410320
- Shahbaz T., 1999, *J. Astrophys. Astron.* Vol. **20**, p. 197

- Stefanescu A., 2003, Anpassung und Einsatz des OPTIMA Photometer zur Messung von GRB-Afterglow-Transienten, Diplomarbeit, Technische Universität München
- Straubmeier C., Kanbach G. and Schrey F., 2001, *Experimental Astronomy*, Vol. **11**, p. 157
- Szkody, P., Scott F., Agueros M. et al., 2002, *Astron. J.*, Vol. **123**, p. 430
- Szkody, P., Scott F., Schmidt G. et al., 2002, *Astrophys. J.*, Vol. **583**, p. 902
- Taylor C.J., Thorstensen J.R. et al., 1999, *Publ. Astron. Soc. Pacific*, Vol. **111**, p. 184
- Tovmassian G.H., 2004, astro-ph/0412239
- Van der Klis, M., 1989, *Annu. Rev. Astron. Astrophys.*, Vol. **27**, p. 517
- Van der Klis, M., 2000, *Annu. Rev. Astron. Astrophys.*, Vol. **38**, p. 717
- Warner B. 1988, *High Speed Photometry*, Cambridge Univ. Press
- Warner B. 2004, *Publ. Astron. Soc. Pacific*, Vol. **116**, p. 115
- Wiehahn M., Potter S.B., Warner B., et al., 2004, *Mon. Not. R. Astron. Soc.*, Vol. **355**, p. 689
- Wijnands R., 2000, astro-ph/0008096
- Woudt P.A., Warner B. and Pretorius M.L., 2004, *Mon. Not. R. Astron. Soc.*, Vol. **351**, p. 1015

Appendix A

Programs

During the data analysis constructions of light curves, correlation functions and power spectra were made. Existing transforms in SigmaPlot were used as well as constructed programs in MATLAB and SigmaPlot to produce the diagrams.

A.1 Light Curves

The light curves were constructed by a reduction of the data from the original intensity files of the sources and the background sky. This was done in MATLAB and/or SigmaPlot. The intensity file consists of segments containing a number of channels depending on which mode was used. For each segment, values are put in the 24 first channels and the remaining channels are filled with zeros. A program was constructed in SigmaPlot to select the 24 first channels in each segment. Data are collected in a channel during the time interval 0.04194304 s corresponding to 1/24 s, and successive channel values were incremented by this value to get a sample-time x-axis *figure A.1*.

A.2 Power Spectra

A.2.1 SigmaPlot

The routine in *figure A.2* was used to retrieve power spectra by the program *POWSPEC.XFM* in SigmaPlot. Input data were segments of intensity traces, corrected for the background intensity level. The data sets were of length 2^N where N is an integer. The program includes an optional use of a *Hanning window*, a function that drops to zero at each end of the data segment.

A.2.2 MATLAB

Power spectra were in some cases constructed in MATLAB by using the function *fft* and then calculates the power spectra as the square of the Fourier transform, $(\text{abs}(\text{fft}(\text{Intensity})))^2$. The program *SimCalc* was constructed by Ricky Nilsson to simulate the expected correlation function and power spectra from known light-curves *figure A.3*.

```

'Light-curve Extractor
'This transform extracts the 24 first channels in each segment of the input file.
'Import the file from row 22. Segment 1 has values from row 1 –512. The following segments
'consist of 10 rows of text and 511 rows of values. Each segment is filled with zeros after the
'24 first channels.
'Column 2 is the output file.

x=2000 'sample time

for sec=1 to (x +1) step 1 do
i=1+(sec-1)*522
col(4,(1+(sec-1)*24),(1+(sec-1)*24)+23)=col(2,i+23))
end for

'The zeros are removed using the function “SigmaStat Transforms” –“Filter”.
'”Upper bound” should be put to “infinity”.
'”Lower” should be put to 0.1.

'This transform creates an x-axis time scale that is put in column 7.

y=col(5) 'Input file

length=size(y)
nx=data(1,length,1)
col(7)=0.04194304*nx

```

Figure A.1: *The program Light-curve Extracter constructed in SigmaPlot was used to create the light curves.*

```

' Power Spectral Density
'   This transform computes the power spectral density (psd) of
'   the data in column ci and places it in column co
'       If a nonzero sampling frequency fs is specified then a frequency
'       axis is placed in column co with the psd in the next adjacent
'       column
'       If han = 1 then a Hanning window is applied to the padded data
'       Set Trig Units to Radians

' Input
ci = 1      ' input column number
co = 2      ' first output column number
fs = 24     ' sampling frequency (produces frequency axis if fs > 0)
han = 1     ' Hanning window (1 = use; 0 = don't use)

' Program
pi=3.1415926
x1 = col(ci)
if han = 1 then                                'use Hanning window
    n=size(x1)
    nlog2=log(n)/log(2)                        ' pad data if necessary
    powup=int(nlog2)
    intup1=f(nlog2-powup < 1e-14; 2^powup; 2^(powup+1))
    rl=f(mod(n,2)>0; (intup1-n+1)/2; (intup1-n+2)/2)
    ru=if(mod(n,2)>0; intup1-rl; intup1-rl+1)
    x=if(rl-1>0; if(intup1-ru>0; {data(0,0;rl-1);x1;data(0,0;intup1-ru)}; {data(0,0;rl);x1});
        if(intup1-ru>0; {x1;data(0,0;intup1-ru)}; {x1}))
    w=.5*(1-cos(2*pi*data(0,intup1-1)/(intup1-1)))
    xf=w*x                                      ' multiply padded data by window
else
    xf=x1
end if

tx = fft(xf)                                    ' fft of data
nf=size(tx)/4                                  ' half the zero padded data length
spec = real(tx)^2 + img(tx)^2                  ' power spectral density
spechalf = spec[data(1;nf+1)]                  ' half the symmetric psd data
f = fs*data(0,nf)/(2*nf)                       ' frequency axis

' Output
col(co) = if(fs>0;f,spechalf)
col(co+1) = if(fs>0,spechalf)

```

Figure A.2: The program POWSPEC.XFM in SigmaPlot creates power spectral density diagram of the input intensity trace

```

%-----By: Ricky Nilsson (2005)-----
%This function (SimCalc.m) will calculate and plot the correlation function and
%power spectrum of the input signal simout1.
function [confunc Xval, Confunc] = SimCalc(simout1, sampletime, periods) %The input
signal and its sample time are specified in
                                %the command prompt,
                                %including the number
                                %of periods you want to simulate.

[i,j,simout1] = find(simout1);      %If the signal is padded with zeros, this will
truncate the vector.
Lightcurve = simout1';              %Transpose to row-vector.
n1 = length(Lightcurve);            %Determine number of elements in Lightcurve
vector.

Xmax = (sampletime)*(n1-1);          %Convert to correct values on Lightcurve x-
scale.
lightcurveXval = [0:sampletime:Xmax];
subplot(3,1,1)                      %Activate subplot.
plot(lightcurveXval, Lightcurve), title('Lightcurve'), xlabel('Time t [s]'), ylabel('Intensity
[arbitrary units]')

PerLightcurve = repmat(Lightcurve,1,periods); %Repeat Lightcurve (number of
periods).
n2 = length(PerLightcurve);          %Determine number of elements in the periodic
Lightcurve.

Confunc = xcorr(PerLightcurve,'unbiased'); %Calculate the correlation function of the
periodic Lightcurve.
n3 = length(Confunc);

Xval = (length(Confunc)-1)/2;         %Center correlation function at x=0.
confuncXval = [-Xval:Xval]*sampletime;
subplot(3,1,2)
semilogx(confuncXval, Confunc), title('Auto-correlation of lightcurve'), xlabel('Delay
time \tau [s]'), ylabel('Auto-correlation <I^2> [arbitrary units]')

%N = floor((log(n3))/(log(2)));
%Confunc(((2^N)+1):n3)=[];            %Truncate correlation function array
to 2^N elements.

Fourier = fft(Confunc);               %Calculate the discrete Fourier transform of the
correlation function.
Fourier(1) = 0;
Fourier(length(Fourier)) = 0;

```

Figure A.3: The MATLAB program *SimCalc* calculates the light curve, correlation functions and power spectra of the input intensity trace

Appendix B

Manual and User Guide for the Digital Correlator *Flex01-05D* and the Control-Program *PhoCorr*

By: Ricky Nilsson & Helena Uthas

B.1 Introduction

This short manual is intended to give a basic introduction to the correlator model Flex01-05D and the software we have developed in the LabVIEW programming environment.

The correlator was purchased in 2002 from the company *Correlator.com* for use in the optics-lab at Lund Observatory.

B.2 Basic correlator specifications

The correlator has two connectors (in-channel A and B) for transferring standard TTL pulses from the system detectors and it can be operated in 3 correlator-modes and one photon history recorder mode.

In all the correlation modes described below an intensity series is also transferred to the host computer via USB. The number of photon pulses within the interval 0.04194304 seconds is registered and divided by the time interval to give the intensity in units of Hz.

B.2.1 Mode A: Single auto/cross correlation

Calculates the auto (AxA) *or* cross (AxB) correlation function and transfers the normalized values for delay times from 5 ns to 23 min in 1088 channels, via a USB cable to the host computer. The first 64 channels contain the values for delay times 5 ns (being the minimum sample time) to $64 \cdot 5$ ns, the next 32 channels contain values for delay times $64 \cdot 5 + 10$ ns up to $64 \cdot 5 + 32 \cdot 10$ ns etc, with sample time doubling every 32 channels. Thus, the delay time for the last channel of every 32-channel segment is given by $5(64 + 32(2 + 2^2 + 2^3 + \dots + 2^n))$ where n is the number of the 32-channel segment. In this mode there are 32 segments, i.e. maximum delay time is 23 min. In addition to the correlation function the intensity series for channel A and B are also transferred to the host computer.

B.2.2 Mode B: Quad correlation

Calculates the auto (AxA and BxB) *and* cross (AxB and BxA) correlation functions and transfers the normalized values for delay times from 5 ns to 23 min in 288 channels for each function. The first 16 channels contain the values for delay times 5 ns (minimum sample time) to $16 \cdot 5$ ns, the next 8 channels contain values for delay times $16 \cdot 5 + 10$ up to $16 \cdot 5 + 8 \cdot 10$ ns etc, with sample time doubling every 8 channels. Delay time for last channel of every 8-channel segment (total of 34 segments) is $5(16 + 8(2 + 2^2 + 2^3 + \dots + 2^n))$.

B.2.3 Mode C: Dual auto/cross correlation

Calculates the auto (AxA and BxB) *or* cross (AxB and BxA) correlation functions and transfers the normalized values for delay times from 5 ns to 183 min in 608 channels for each function. The first 32 channels contain the values for delay times 5 ns (minimum sample time) to $32 \cdot 5$ ns, the next 16 channels contain values for delay times $32 \cdot 5 + 10$ ns up to $32 \cdot 5 + 16 \cdot 10$ ns etc, with sample time doubling every 16 channels. Delay time for last channel of every 16-channel segment (total of 36 segments) is $5(32 + 16(2 + 2^2 + 2^3 + \dots + 2^n))$.

B.2.4 Photon history recorder

Used as a photon history recorder the correlator transfers the time differences between successive photon events to the host computer hard drive. You can select to record the photon stream from either channel A or both channel A and B.

B.2.5 Calculating the correlation functions

The correlator uses the multiple tau method to calculate high resolution correlation functions, which means that sample and delay times are varied (in this case doubled) in consecutive channel segments giving a wider temporal range of the correlation function for a single measurement. Thus the correlator uses so called MT-64, MT-32, and MT-16 schemes in mode A, B and C respectively, as described above. The number of photon counts within the sample time represents the intensity within the specific bins. By multiplying intensities of two bins differing in time by an amount equal to the delay time in question and adding the products of all the pairs of multiplied bins, a raw value of the correlation function at this delay time is calculated. The values are then normalized according to two different schemes; symmetric normalization for late delay channels and asymmetric normalization for early delay channels.

Symmetric normalization: The value of the correlation function for a given sample time τ and delay time T is

$$Corr(T) = \frac{\frac{\sum_{i=1}^N A_i \cdot B_{i+T/\tau}}{N}}{\frac{\sum_{i=1}^N A_i}{N} \cdot \frac{\sum_{i=1}^N B_{i+T/\tau}}{N}} \quad (B.1)$$

where $\{ A_i, i = 1 \text{ to } N + T/\tau \}$ and $\{ B_i, i = 1 \text{ to } N + T/\tau \}$ are the intensity series and N is the number of elements. The summation in the numerator represents the raw correlation function value. In the denominator the average intensity for A is multiplied with the average delayed intensity for B. This is not the case in the asymmetric scheme.

Asymmetric normalization: Here the value of correlation function is given by

$$Corr(T) = \frac{\frac{\sum_{i=1}^N A_i \cdot B_{i+T/\tau}}{N}}{\frac{\sum_{i=1}^N A_i}{N} \cdot \frac{\sum_{i=1}^N B_i}{N}} \quad (\text{B.2})$$

The result is the same as in the symmetric scheme when $T/\tau \ll N$. For larger delay times compared to N , the symmetric normalization reduces noise as shown by Klaus Schätzel [1], [2], [3] and [4].

B.3 LabVIEW

LabVIEW is a graphical programming language produced by National Instruments. Two different windows are used; The *front panel* is the user interface and it is used for data displaying and for controlling different functions that are programmed on the block diagram. The *block diagram* is where these functions and objects are linked together with wires. Different tools as function palette and tool palette are used to produce the different functions.

The possibilities of making programs for special applications in LabVIEW are many, but LabVIEW is mainly used for controlling an external instrument.

For further information; www.labview.com

B.4 Flexx01

A couple of sample programs in *VB (Visual Basic)*, *C++* and *LabVIEW* were provided for programming the correlator, and for our interests, the sample program *Flexx01* was a good start for programming in LabView. The following describes what this sample program consisted of and its basic functions. The program communicates with the correlator by calling specific library functions in the *flex01-05d.dll*-file. The functions are listed below with some explanations of what they do and which output parameters that are required.

All functions, *USB Initialize*, *Start*, *Update*, *Stop* and *Free* are organized in a *Stacked Sequence Structure* and they will execute in a specific order. The USB Update is placed in a *For Loop* that will execute N times before it continues with the stacked sequence structure. A function *Wait* is placed inside the For Loop and it will wait a given number of milliseconds before the For Loop runs again.

B.4.1 USB Initialize

mode A (Single correlation) = 65

mode B (Quad correlation) = 66

mode C (Dual correlation) = 67

This function is called by a *Call Library function node* on the block diagram and it is initialized by the input values above depending on in which mode you want to run the correlator. The input signal to the Call library function is of type numeric and data type unsigned 8-bit integer.

B.4.2 USB Start

Auto = 1 and Cross = 0 (only for single and dual mode)

A Boolean (false or true) from the auto/cross button is converted to 0 or 1 and wired to the input parameter of USB Start. The value sent to this library function node will decide if the specified mode calculates the auto or cross correlations.

B.4.3 USB Update

To get correlation functions and intensities you need to call the function USB Update. There are some parameters of different data type corresponding to the different outputs of the function; elapsed time, trace count, intensity trace A and B and the correlation functions.

- Elapsed Time starts counting the time as soon as USB Start is called. It is of numeric type and the data type, 4-byte single.
- Trace Count counts the number of new trace values. The number depends on the specified number of milliseconds in the function Wait. It is of numeric type and data type unsigned 16-bit integer.
- Correlation function 1-4, intensity trace A and trace B are of array type and data type 4-byte single. The arrays which are going to contain the correlation functions, trace A and trace B are created and initialized with zeros and sent as input parameters to USB Update. The corresponding output parameters are pointers to the different arrays and these are sent to an indicator display. The dimension size of the array for the different parameters are;
 - Correlation 1: 1088 elements
 - Correlation 2: 608 elements
 - Correlation 3 and 4: 288 elements each
 - Trace A and B must have array sizes at least equal to the trace count which depends on the time set in the Wait function in the For Loop.

In single mode correlation 2, 3 and 4 are ignored and in dual mode correlation 3 and 4 are ignored.

B.4.4 USB Stop

This function will stop the signal.

B.4.5 USB Free

Is called to clean up before exit.

B.5 PhoCorr

Based on the sample program Flexx01 which was designed only to run in single mode and without any graphical representation of the measured correlation functions and intensity series, we have developed a more flexible LabVIEW program which can run the correlator in all the specified modes and display correlation functions and intensity series in graphs. The program also saves the obtained data in a txt-file for further analysis e.g. calculation of power spectra. For the *Photon History Recorder mode* a separate program, called *Photon*, is used since the DLL-file (flex01-05d.dll) written for use with LabVIEW lacks this function.

B.5.1 Interpreting the block diagram

For possible future modification of the program and easier interpretation of the block diagram a short description of the latter is presented in the following section. The basic structure is as mentioned earlier, a Stacked Sequence, and the functions in the different sequences will therefore be presented separately. For further information and detailed explanations of how to program in LabVIEW the user is referred to www.labview.com or other online LabVIEW tutorials.

Sequence 0: The correlator is initialized with the corresponding value of the chosen mode. This value is also passed on to the next sequence.

Sequence 1: Contains the main part of the program code enclosed by a *While Loop* which runs until elapsed time reaches the specified run time. The wait function is set to 1000 ms. During this time the correlator gathers intensity trace values and calculates correlation functions which are transferred to the computer when USB Update is called in the next iteration. Since it takes some time to run the subdiagram the actual run time might exceed the specified with a few tenths of a second as the final iteration finishes. Initially the Library function USB Start is called (outside the loop) and it starts the correlator in dual or cross mode.

The 8 output parameters from USB Update are as mentioned; elapsed time, trace count, correlation function 1 (corr1), corr2, corr3, corr4, intensity trace A and intensity trace B, in that order. Data from these parameters are wired to different subVIs which are subprograms (VI-files just like the main VI *PhoCorr.vi*, *Figure B.3*) saved in the same folder as the main VI. Each subVI is shown as a connector pane with a set of input and output terminals that correspond to the controls and indicators of that VI. The intensity traces A and B are sent to *intensityAsub.vi* and *intensityBsub.vi* respectively. These subVIs (*Figure B.1*) also include a function that saves the intensity trace values in files named *intensityA.txt* and *intensityB.txt*. Feedback nodes are employed to transfer new trace values from one iteration to the next. The new trace values are appended to another array which grows in size with the added elements each iteration. Array indices are translated to elapsed time in the graph axis settings in the mode subVI that receives the intensity data.

Singlesub.vi, *Dualsub.vi* and *Quadsub.vi* are placed inside separate Case Structures and are thus executed and launched as separate front panels only if the selected mode number corresponds to 65 (in case of Single), 66 (in case of Quad) or 67 (in case of Dual).

In the block diagram of *Singlesub.vi* (*Figure B.2*) the arrays of intensity values for channel A and B are wired to waveform graphs which are displayed in the front panel. The array containing correlation function values are sent to yet another subVI, *singlecorrfunc1sub.vi*, in which the channel index is replaced with the corresponding delay time values as x-values and sent to a XY-graph. In this subVI the values of the correlation function are also saved to a file named *singlecorrfunc1.txt*. Besides the correlation function and intensities, the elapsed time and

number of new trace values are wired to numeric indicators and displayed on the front panel of the subVI. The subVIs for Dual and Quad mode are built up in a similar way, but obviously with a different number of correlation functions and related delay times.

Sequence 2: The correlator is stopped.

Sequence 3: The correlator is “cleaned up” and the latest channel values are removed.

B.5.2 How to use PhoCorr

When starting the program PhoCorr a front panel containing a short list of how to run the program is shown. Start by choosing mode from the list (single, quad or dual) and then choose auto or cross correlation. Specify run time and then press the white arrow (run button) in the subVI menu bar. A new window opens that show correlation functions and intensity traces. In the left frame, elapsed time, number of new trace values and amplitudes for intensity traces and correlation functions are shown. Change the plot range by writing new values directly into the graph or use the *Graph Palette*, on top of the graphs, to activate the zoom function. Make sure you have disabled this function by pressing the zoom button again when finished resizing. Pressing the white hand on the Graph Palette makes it possible to move the graph.

On top of the correlation functions is a *Cursor Legend*. Specific graph positions can be marked and the exact x and y values can be acquired. Choose *Bring to center* or *Go to cursor* in the cursor menu to make a cursor. The first brings the cursor to center position of the graph and the second moves the graph to the cursor. The cursor can be moved when the *cross button* is chosen in Graph Palette or by clicking up/down/left/right in the directional button (a white and blue square). Cursor style as colour and linewidth can be chosen in the menu. Lock the cursor to a specific position by choosing *Lock to plot* in menu. To get multiple cursors change to edit mode in the subVI menu *Operate >> Change to Edit mode* and choose *Show Tools Palette* from *Window*. A toolbox will appear. Use the arrow to enlarge the cursor window, and more Cursor Legends will appear depending on window size. Change to run mode again when finished, *Operate >> Change to Run mode*. To choose visible items such as *Plot Legend*, *x-scrollbar* or autoscaling, right click on Graph palette and a menu will appear.

Interrupt the running process by pressing the red button situated on the subVI menu bar. Remember to rename the saved files after each execution to keep them from being overwritten when the program is run again. Alternatively change the save settings in the *Write LVM File function* on the specific subVI block diagram by clicking *Operate >> Change to Run mode* and then double click on the function icon.

Bibliography

- [1] Klaus Schätzel, *Single Photon Correlation Techniques*, Dynamic Light Scattering: The method and some applications, edited by Wyn Brown, Clarendon Press, Oxford, p. 76, 1993.
- [2] Klaus Schätzel et., *Noise in Multiple-Tau Photon Correlation Data*, SPIE Vol. 1430, p.109, Photon Correlation Spectroscopy: Multicomponent Systems, 1991.
- [3] Klaus Schätzel, *New Concept in Correlator Design*, Inst. Phys. Conf. Ser. No. 77, p. 175, 1985.
- [4] Klaus Schätzel et., *Photon Correlation Measurements at Large Lag Times*, Journal of Modern Optics, Vol. 35, No. 4, p. 711, 1988.
- [5] *Getting started with your new Flex01-05D USB based Digital correlator*, Correlator.com, 2004

B.6 Appendix

The figures referred to in the text are presented on the following pages.

Figure 1: Block diagram of intensity A subVI.

Figure 2: Block diagram of single correlation subVI.

Figure 3: Main block diagram

Figure 4: Front panel of single cross-correlation run.

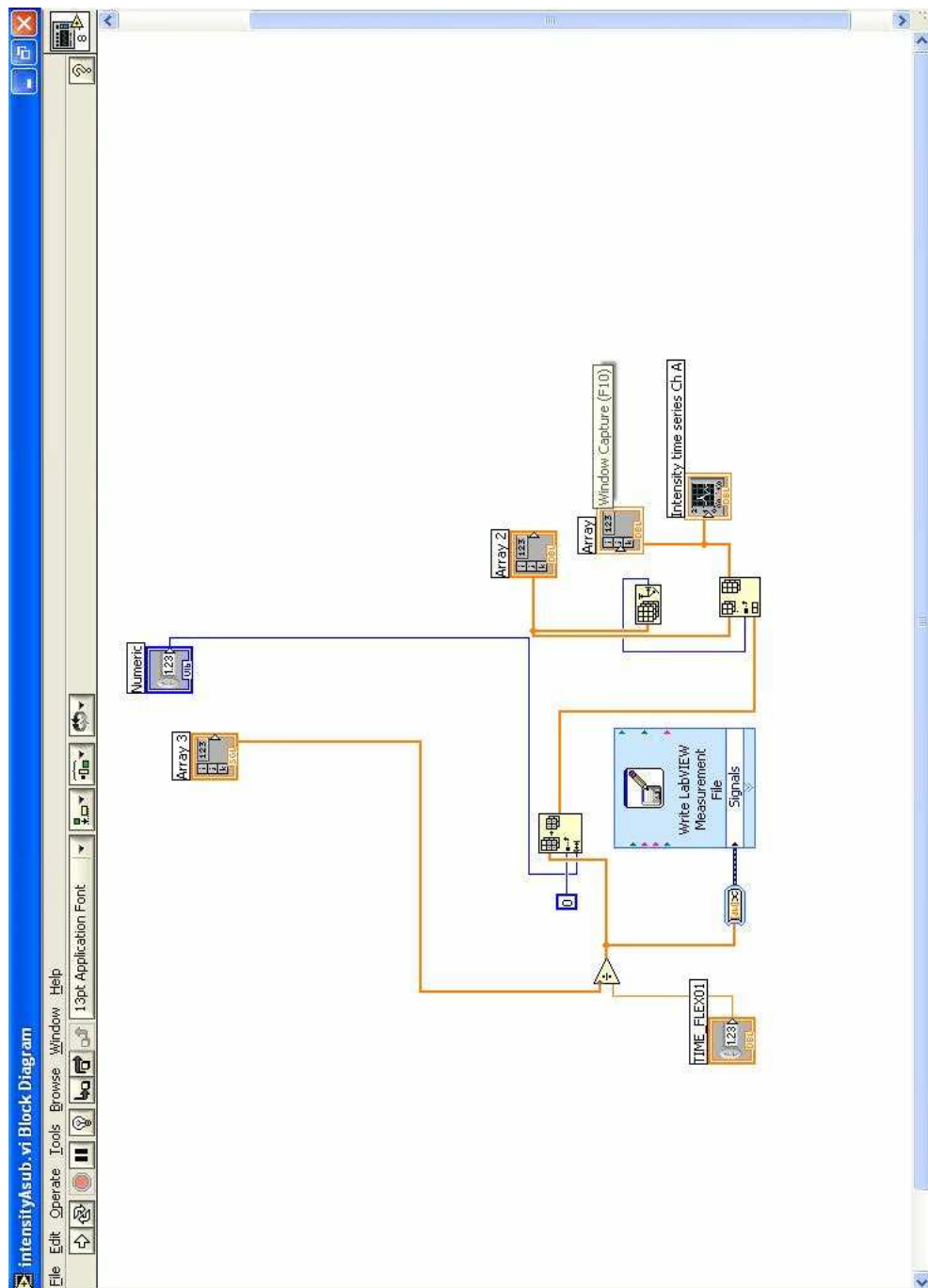


Figure B.1: Block diagram of intensity A subVI.

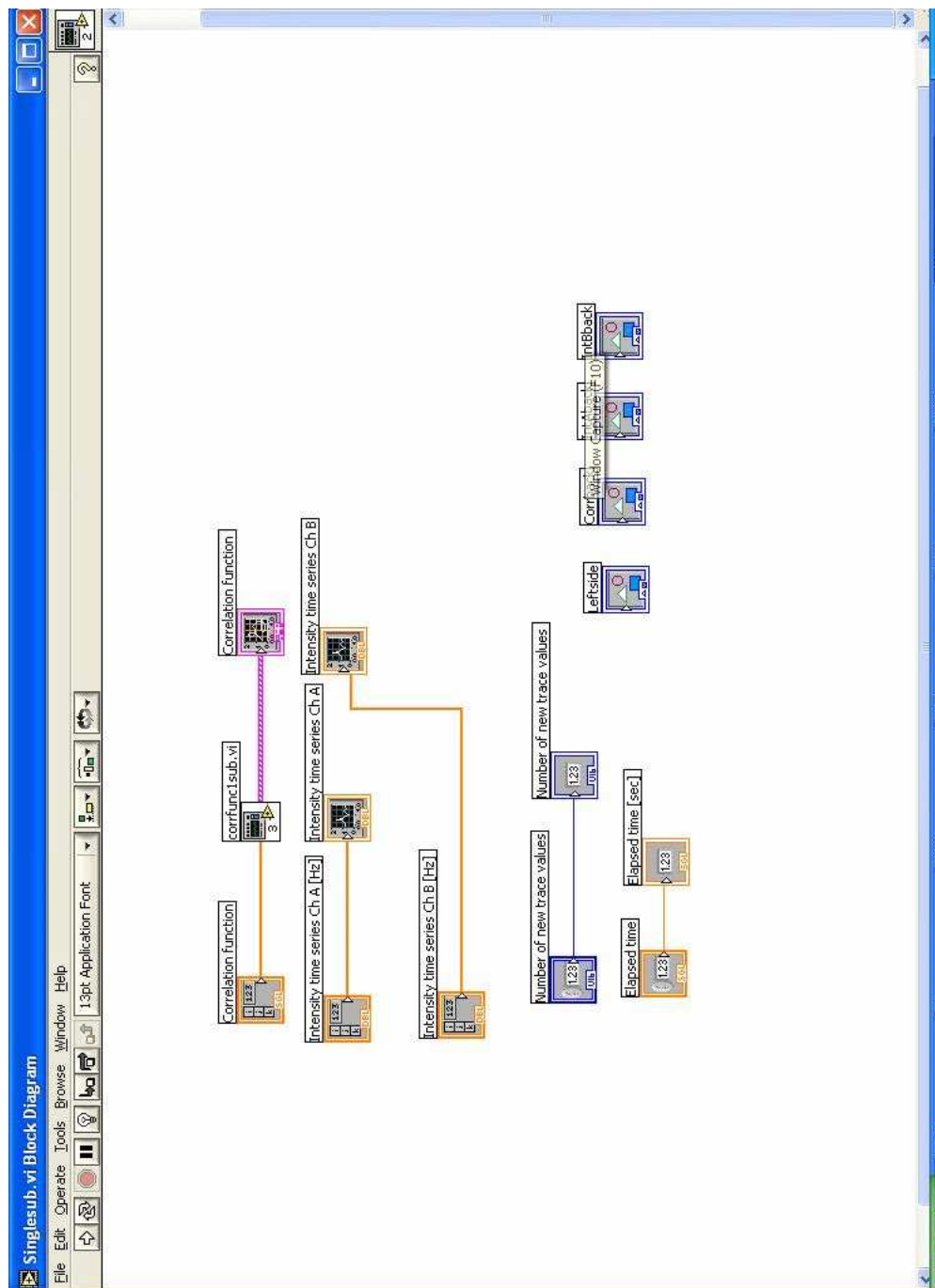


Figure B.2: *Block diagram of single correlation subVI.*

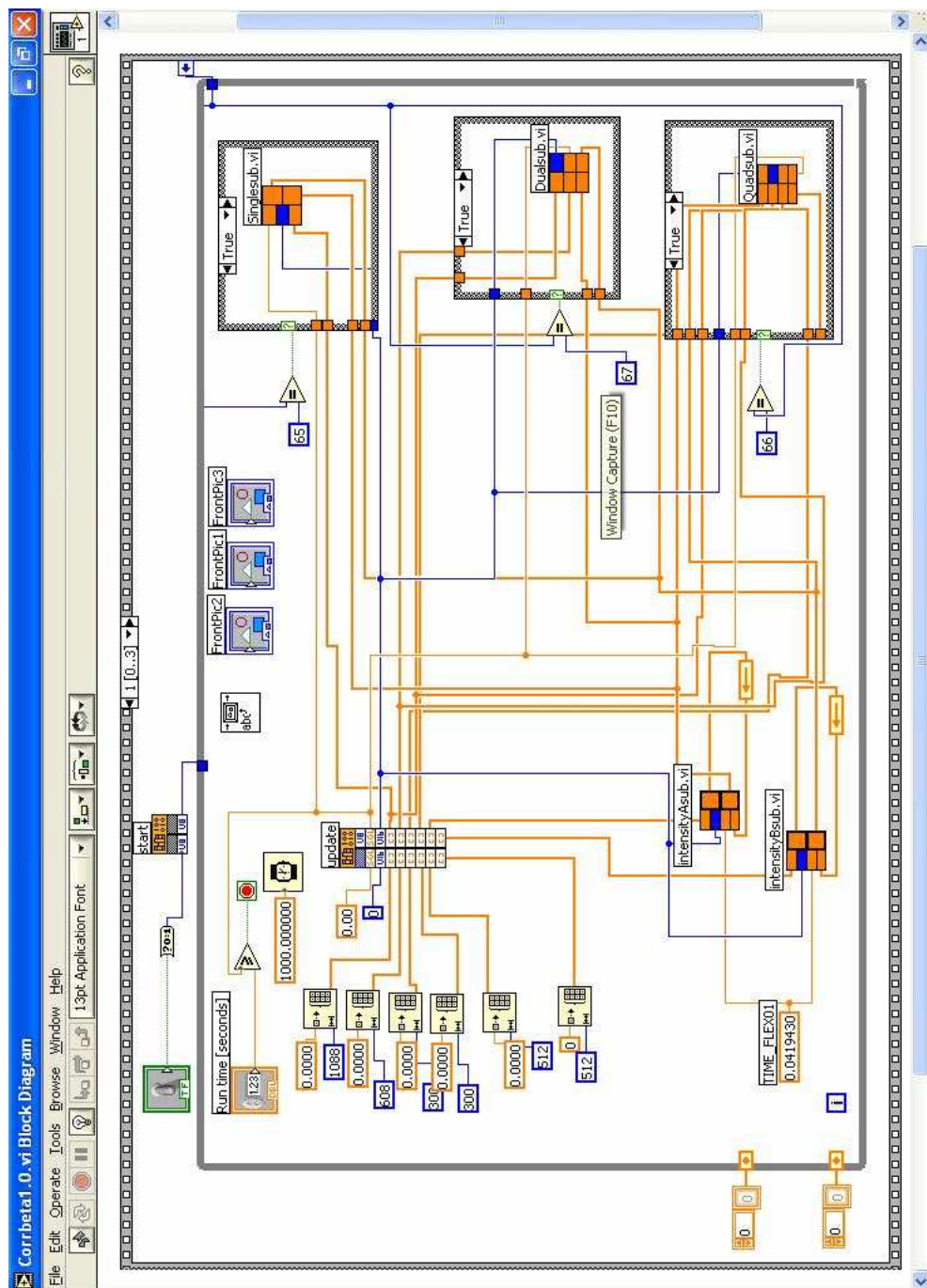


Figure B.3: Main block diagram

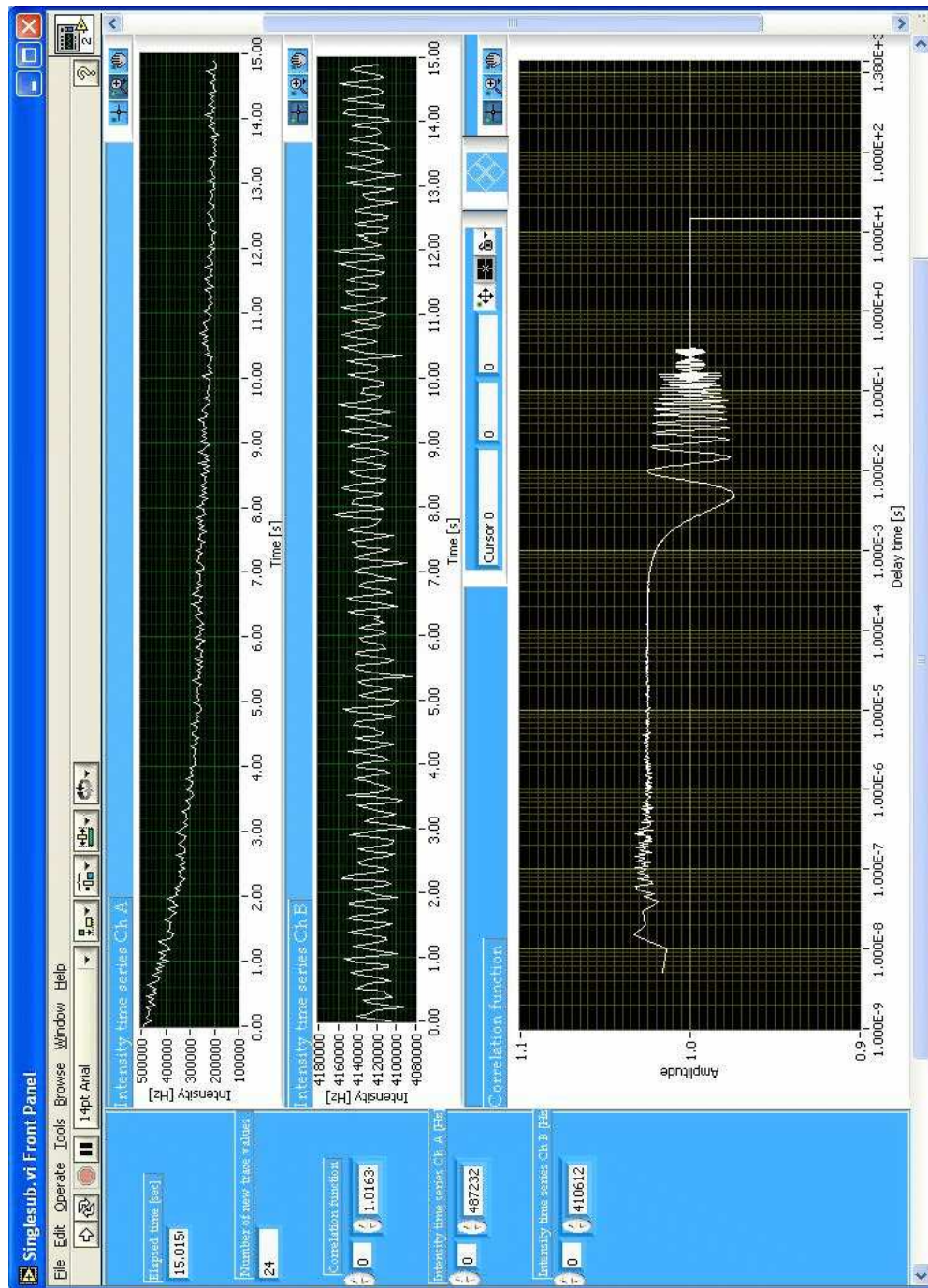


Figure B.4: *Front panel of single cross-correlation run.*